SOLUTION PROCESSED OPTICAL COATINGS

FOR SOLAR CELL APPLICATIONS

by

RAJESH TUMMALA

Presented to the Faculty of the Graduate School of

The University of Texas at Arlington in Partial Fulfillment

of the Requirements

for the Degree of

MASTER OF SCIENCE IN MATERIAL SCIENCE AND ENGINEERING

THE UNIVERSITY OF TEXAS AT ARLINGTON

MAY 2009

ACKNOWLEDGEMENTS

First of all, I would like to thank my thesis advisor Professor Weidong Zhou, who gave me this great opportunity to work and perform research in his Nanophotonic Device Research Group. Even though I had a very little knowledge in the field of optical coatings and design, he constantly guided and encouraged me. Without his guidance and support, I would not have been able to finish this thesis.

I am very grateful to Dr.Yuehui Wang for her guidance and contribution throughout this thesis work. I would like to thank Li Chen for his cooperation to perform optical design. I also thank other group members of Nanophotonic Device Research Group for their guidance and cooperation. Special thanks to Professors Meng Tao and Michael Jin for their suggestions and guidance throughout this thesis work and also for accepting to be in my thesis defense committee.

I would like to thank NanoFab, the nanotechnology research and teaching facility, for giving training for high technology equipment, and for giving suggestions whenever required.

I am very thankful to friends Srinivasa Narsimhan Chakravarthy, Alex Alphonse, Yi Yang, Naga, Datta, Megha, Subbaraju, Joga Rao, Laxman, Zeenath Reddy and Durga for their support and encouragement throughout my Masters degree.

Last but not least, I would like to express my honest gratitude to my parents and god for giving me strength, love, motivation and blessings throughout my life. I would also like to thank Madhusudhana Rao - my cousin, my sister and brother-in-law for their support and encouragement.

April 24, 2009

ABSTRACT

SOLUTION PROCESSED OPTICAL COATINGS FOR

SOLAR CELL APPLICATIONS

Rajesh Tummala, M.S.

The University of Texas at Arlington, 2009

Supervising Professor: WEIDONG ZHOU

In the recent past the demand for higher energy conversion efficiency of solar cells is on the rise. Extensive research is carrying out and many new methods have been proposed by changing either fabrication process or implementation of anti-reflection coatings. In this thesis, the solution processed omni directional anti-reflection coatings have been demonstrated on commercial amorphous silicon solar cells and on fabricated organic solar cells. A simple convective coating technique is utilized to deposit spherical silica micro-particles on the commercial amorphous silicon solar cells and on fabricated organic solar cells. In order to investigate the behavior of solar cells at different times of the day, we have measured the output electrical parameters of the solar cell at different angles of light incidence from 0^o to 60^o with a home built set up. It was found that spherical surface texture reduces the reflectivity in the wavelength regime of 400-1200 nm and efficiency enhancement was also observed at all angles of light incidence and as high as 12% was achieved at larger incident angles. This method proved to be very cost effective because of the use of simple deposition techniques and easy way of processing. Another technique, dip coating process, has also been studied to obtain inorganic dielectric particle based Distributed Bragg Reflectors (DBR) for applications in one-dimensional photonic crystal, and in resonance cavity photonic devices. The properties of

the fabricated DBR structures were characterized with reflection measurement and other structure characterizations. All these convective coating and dip coating processes enable simple fabrication of optical structures for novel photonic device applications.

TABLE OF CONTENTS

LIST OF ILLUSTRATIONS

LIST OF TABLES

CHAPTER 1

INTRODUCTION

Photovoltaic devices such as solar cells work on the principle of converting light energy from sun into electrical energy. When the photons with sufficient energy penetrate into the semiconductor, excite the electrons from valence band to conduction band generating electric current. One of the key issues of solar cell devices is the low energy conversion efficiency. Although many anti-reflection methods like surface texturing and a thin film of transparent conducting oxide are being used, a more cost–effective method is needed where anti-reflection methods improve efficiency by not changing the microelectronics fabrication methods or by altering the device chemistry. By the application of advanced materials chemistry and optical design, energy conversion can be improved [1, 2, and 3]. This approach motivated us to implement some principles of colloids, solution processing with simple deposition techniques like convective coating, spin coating and dip coating. This thesis is about application of solution processed colloidal particles using above mentioned deposition techniques for anti-reflective coatings on commercial amorphous silicon solar cell and fabricated organic solar cell and also for fabricating Distributed Bragg Reflectors (DBR).

1.1 Overview of Colloids

Any particle that has some linear dimension between 10^{-9}(nano)–10^{-6}(micro) is considered as colloid. The colloidal particles dispersed in liquids exhibit astonishing properties. The particles of a dispersed suspension are only suspended in the mixture where as in a solution they are completely dissolved. The particle size and shape are of considerable importance in the properties of a colloidal system. The simplest shape, a sphere, is a characteristic of emulsions, lattices, and gold and silica sol-gels. Primarily colloidal assembly

offers two advantages; first it typically does not require energy intensive high technology deposition techniques, secondly the forces that govern colloidal assembly are all naturally occurring physical phenomenon. The other advantage is that their scale bridges the molecular and macroscopic worlds as shown in figure 1.1, such small size scales often give novel physical properties where they have numerous applications in the field of photonic crystals, optoelectronic devices and coatings, telecom applications, light emitting materials, sensors etc,.[5]

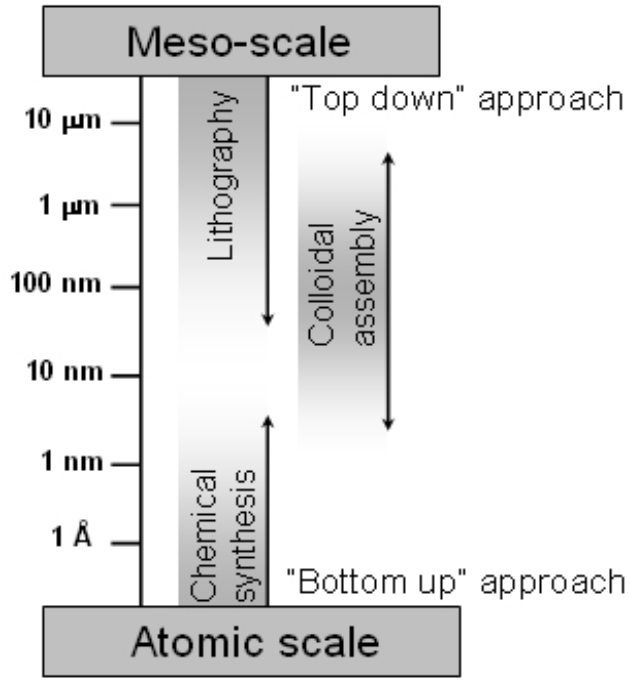

Figure 1.1 Illustration of the size scales for colloid assembly between lithography and chemical synthesis techniques [5]

Colloidal particles are influenced by different intermolecular and surface forces which govern the formation of different structures. Temperature and pressure also plays an important role by depositing with different techniques to get an ordered structure as shown in figure 1.2.

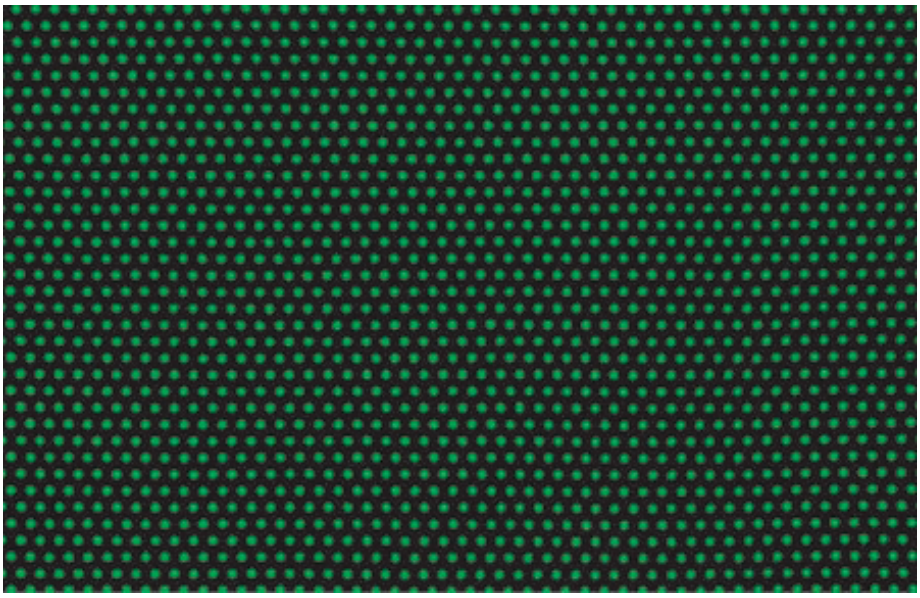

Figure 1.2 N-isopropylacrylamide (NIPA) colloidal particle crystal, Science cover page (August – 2005)

1.2 Deposition Techniques

Different deposition techniques have been developed to deposit colloidal based materials especially in liquid phase. Traditionally various vacuum-based and chemical etching processes have been used for producing different types of surface structures. In our work convective coating technique is utilized to make anti-reflective coating on commercial amorphous silicon solar cells and on fabricated organic solar cells. Dip coating is used to fabricate Distributed Bragg Reflectors (DBR). Whereas spin coating is especially utilized to deposit the dielectric film spin-on-glass (SOG) after convective coating of silica micro particles. In this section a brief description of convective and dip coating assembly is done.

1.2.1 Convective Coating

Convective assembly was developed originally for controlled deposition of micro- and nano-particles by Denkov et al [6], and further modified for a more scalable device by Prevo and Velev[5]. It works on the principle of solvent evaporation leading to the flow of suspension where

particles are subjected to self assemble onto a substrate in an ordered way at controlled temperature and pressure. Thin structured micro- and nano-particle layers were deposited by dragging the meniscus of micro liter suspension droplets trapped between two plates at constant velocity, as shown in figure 1.3

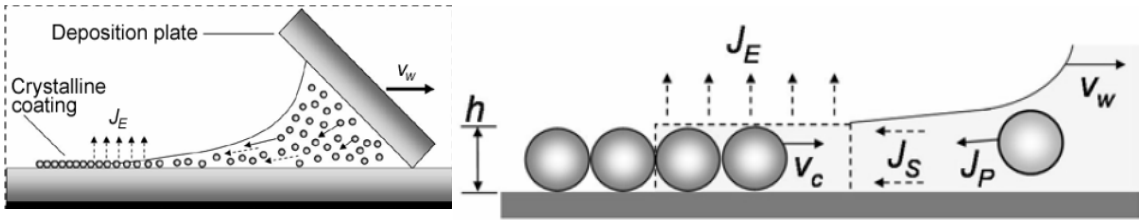

Figure 1.3 Schematic picture of thin wetting drying film. The colloidal crystal of thickness 'h' is deposited at a growth rate 'V_c', at a plate velocity of 'V_w'. The volumetric fluxes, J_P, J_S, and J_E are the particle fluxes, the solvent flux, and the solvent evaporation flux, respectively [5]

For steady state assembly a simple equation was proposed by Dimitrov and Nagayama[21], where a mass transient analysis of the drying film region has been developed.

$$v_C = \frac{K\phi}{h(1-\varepsilon)(1-\phi)} \qquad (1)$$

Where *h* is the film thickness, ε is the porosity of the deposited colloidal films, Φ is the volume fraction of the particles in suspension, and *K* is a hydrodynamic parameter. The material fluxes shown in figure 1.3 are the entrant flux of the carrier solvent (J_S), the resulting hydrodynamic flux of the particles (J_P), the evaporation flux of the solvent leaving the drying region (J_E), and the accumulation of particles in the dried film. The steady state flux balance is taken over by controlled dispersed volume that moves at the rate of accumulation of drying particles, which is equal to the rate of colloidal crystal formation, V_C. The other parameter which defines the film formation is coating plate speed V_w and the angle between coating plate and substrate. For a

fixed concentration and wedge angle and by altering the coating plate speed, loosely packed, multi-layers or closely packed films can be formed as shown in SEM images in figure 1.4, where 2 micron silica particles coating is studied in our laboratory set up[8].

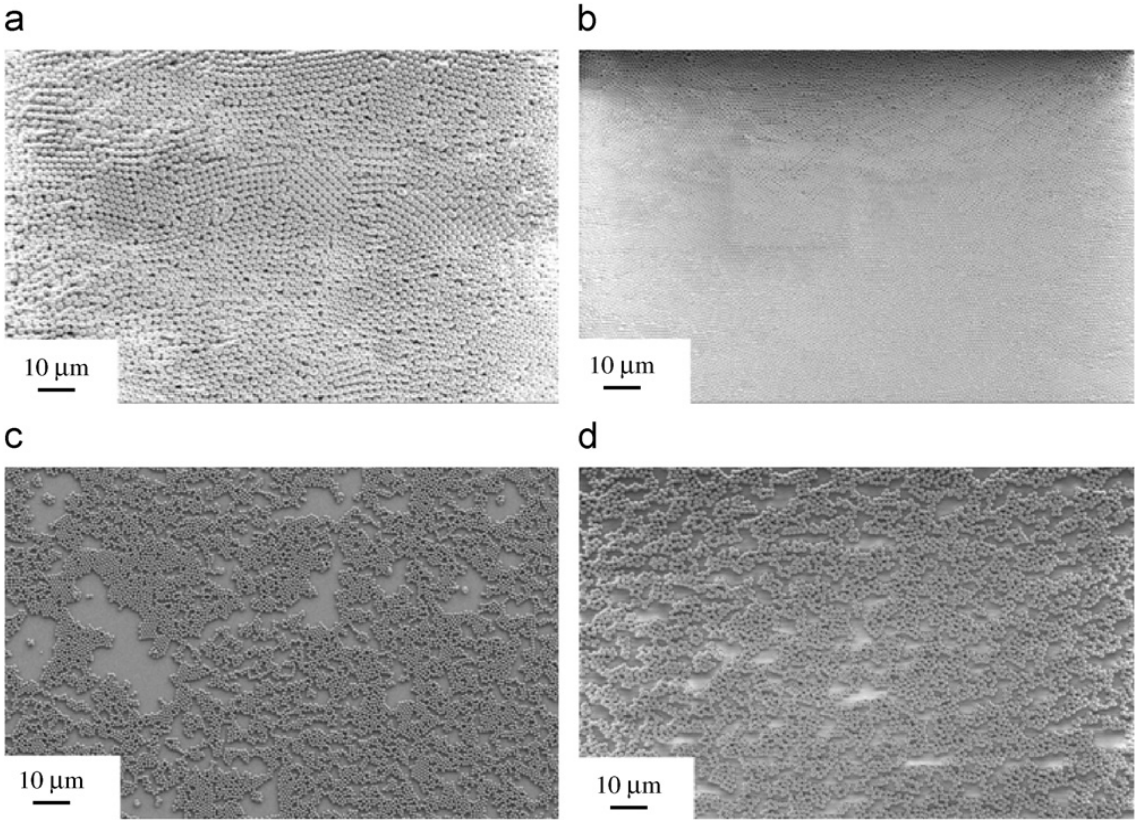

Figure 1.4 SEM images of water-dispersed 2 µm silica spheres at different coating speeds. Other coating parameters are 16 wt% particles concentration, 30 ml dispersed volume and 25^{o} wedge angle on glass substrates (a) 0.02 mm/s (b) 0.04 mm/s (c) 0.07 mm/s and (d) 0.09 mm/s [8]

At 0.02 mm/s large areas of bi-layers and multi layers are formed, where as at 0.04 mm/s uniform monolayer was obtained, with further increase in speed sub-monolayers and loosely packed layers with many clusters of microspheres scattered on the substrate. If the coating plate velocity and the velocity of particle array formation are equal to each other a closely packed monolayer can be formed. If the plate speed is more than the particle formation rate a more loosely packed films are likely to form. On the other hand if the plate speed is lower than particle formation rate, multilayers are likely to form. Along with plate speed the particle

concentration also impacts the type of layers formed. The experimentally determined coating parameters[8] on a 75*25 mm^2 glass substrate to form uniform close packed monolayers at a particular concentration as a function of plate speed (mm/s) and dispersed volume (µL) is shown in figure 1.5.

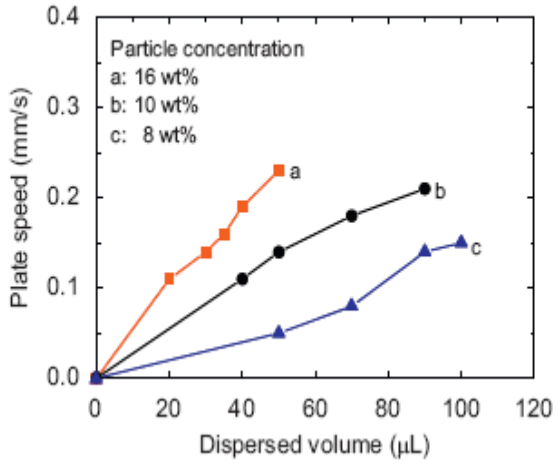

Figure 1.5 Dependence of plate speed on particle concentration in ethanol and on dispersed volume for the formation of large area, uniform, and closely packed monolayers on glass substrate. The concentration of silica microspheres: (a) 16 wt% (b) 10 wt% (c) 8 Wt% [8]

Since the convective assembly is driven by solvent evaporation, selection of solvent is a critical factor in the formation of uniform layers. DI water and ethanol are used as solvents in our experiments to investigate the impact of solvent. The surface coverage of silica microspheres on the substrate is given by $\phi_{sp} = S_{sp} / S$ where, S and S_{sp} represent the total substrate area and the area of the substrate covered by the silica microspheres respectively. The relation between surface coverage and plate speed obtained with 80 µL of water, 30 µL of ethanol as solvent, 25^{o} wedge angle and at 16 wt% particle concentrations is shown in figure 1.6. As the plate speed is increased, ϕ_{sp} increases first with both the solvent and then decreases. It was found that at lower plate speeds silica micro particles are not deposited onto the substrate, indicating lateral capillary force, convective flux, particle-substrate and particle-particle interactions play important role to form closely packed uniform monolayers.

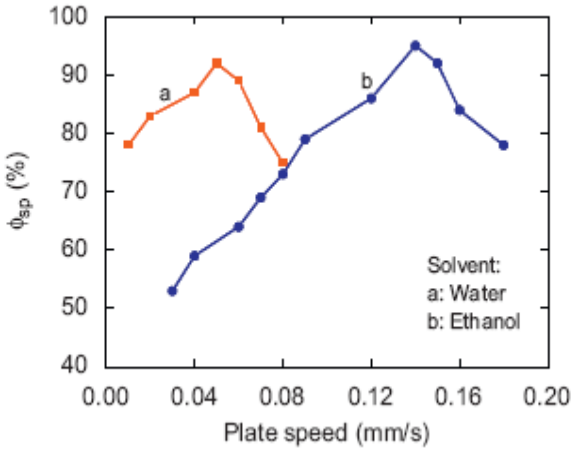

Figure 1.6 Surface coverage as function of plate speed for water and ethanol as solvent [8]

1.2.2 Dip coating

Dip coating technique is a process where the substrate to be coated is immersed in liquid containing colloidal particles and then withdrawn with a well-defined speed under controlled temperature and atmospheric conditions. It is a popular self-assembly process, used to form uniform thin film on a substrate. The substrates could be flat panels, cylinders or complex geometry. One of the features different from convective coating is coating coverage is done on both sides of the substrate and many numbers of ordered layers can be formed on a single substrate as shown in figure 1.7. This process is more advantageous to coat the substrates in the order of square meters, and can also operate in either continuous or batch modes.

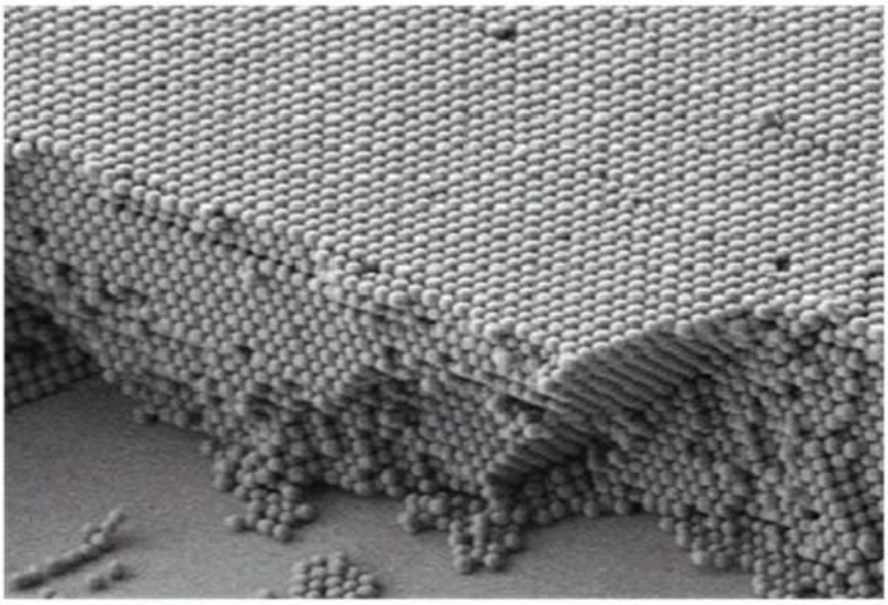

Figure 1.7 Colloid of 1 micron silica micro spheres formed via dip coating [5]

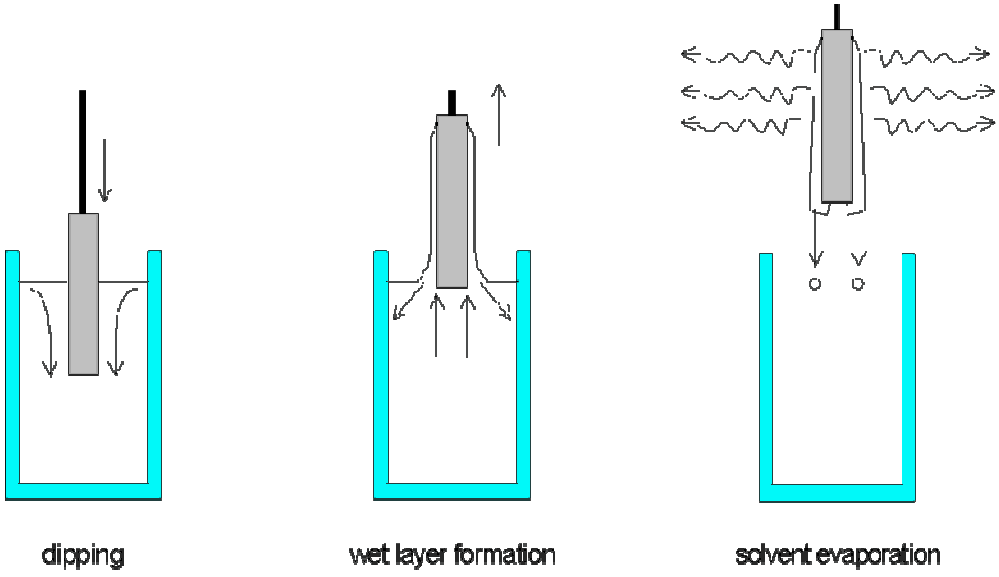

Figure 1.8 Schematic representation dip coating process [11]

The process can be divided into five stages: immersion, withdrawal, deposition, drainage and evaporation[12]. For a coating solution containing volatile solvent, evaporation accompanies the withdrawal, drainage and deposition stage to form a gel film in a relatively short time.

Theoretically thickness of the film produced with this process is determined by different forces acting during different stages of film formation: (1) viscous drag upward on the liquid by the moving substrate, (2) force of gravity (3) resultant force of surface tension in the concavely (4) internal force of the boundary liquid layer arriving at the deposition region (5) surface tension gradient and (6) the disjoining or conjoining pressure. If the substrate speed and liquid viscosity are not high, as is often the case in sol-gel coating processes, the thickness is obtained according to the following relationship[7]:

$$h = \frac{0.94(\eta U)^{2/3}}{\gamma_{LV}{}^{1/6}(\rho g)^{1/2}}$$

Where $\eta, U, \rho and \gamma_{LV}$ are solution viscosity, substrate withdrawal speed, density of solution, and liquid–vapor surface tension respectively. As shown in the figure 1.9 after immersing a clean, wettable substrate into a suspension a self-assembled monolayer is expected to form based on two conditions:

1. Balance between substrate withdrawal rate (V_w) and monolayer array growth (V_c).

2. Balance between evaporation flux of the solvent (J_e) and the entering fluxes of particles (J_p) + solvent (J_w)

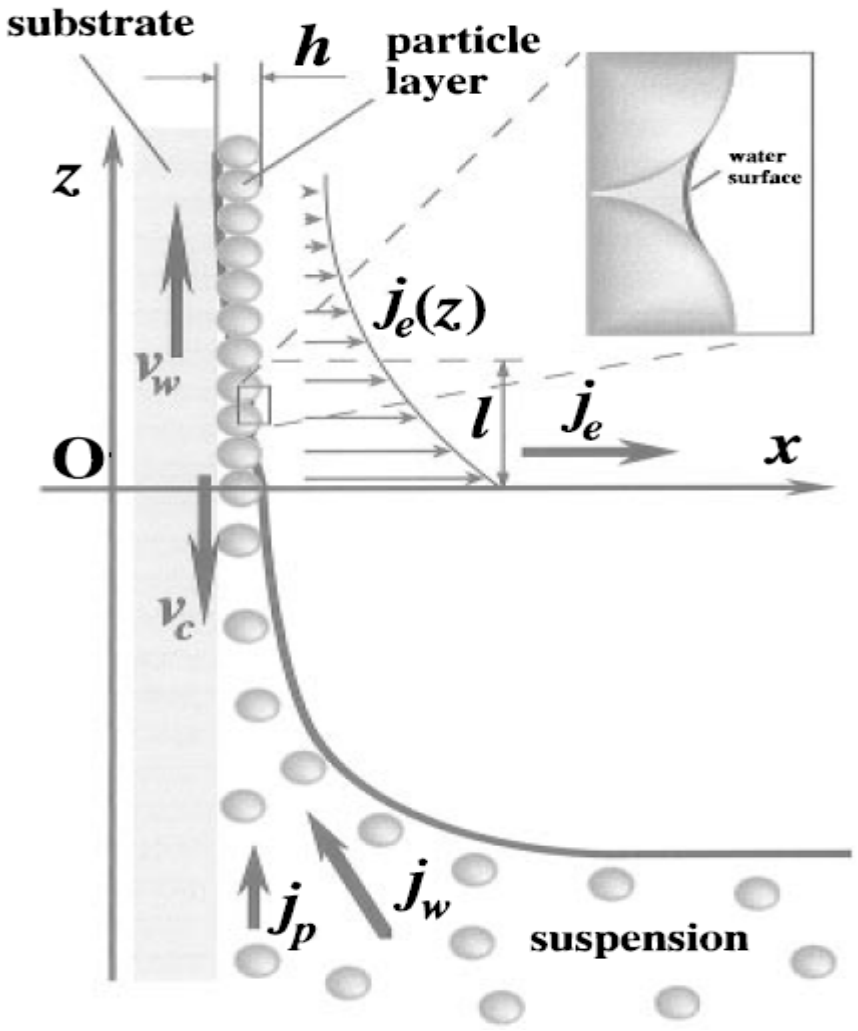

Figure 1.9 Schematic of rates and flux balance. Inset shows meniscus between neighboring particles [21]

The mass-transfer process simultaneously occurs over the entire substrate, ensuring a high process throughput giving well-ordered self-assembled monolayers (SAMs) of nano and micro-particles. The application of SAMs is of practical interest in the area of nanotechnology for example in photonic crystals, optoelectronic devices, sensors and coatings[5, 6, 7and 8]. In this section the process of fabricating Distributed Bragg Reflector (DBR) using Dip Coating technique is demonstrated.

1.2.2.1 Principle of Distributed Bragg Reflector (DBR)

DBR is a reflector of high quality used in waveguides, such as optical fibers. DBR can be formed with multiple layers by alternating materials having different refractive index or by periodic variation of the thickness, resulting in the periodic variation in the effective refractive index in the guide. There is a partial reflection from each layer and a constructive reflection is expected to occur when the product of effective refractive index and thickness is equal to quarter wavelength ($n_{eff} \times thickness = \lambda / 4$). From this equation there is only one wavelength for a particular thickness where light cannot pass. The reflectivity achieved is determined by the refractive index of the layers and the reflection bandwidth is determined by the difference of the refractive index. In this section the DBR are fabricated using dip coating technique on the silicon wafer with 10-15nm silica particles and 10-15nm suncolloid solution which have different refractive indices is demonstrated.

1.2.2.2 Experimental

The materials silica (10-15nm) with IPA as solvent and sun colloid (10-15 nm) with methanol as solvent was used as supplied by Nissan Chemical industries Ltd,. Silicon wafers were supplied by Nova Electronic Materials Ltd. Suncolloid is a colloidal solution containing stannic oxide-zirconium oxide-antimony oxide. Silicon wafers were cleaned with acetone, iso-proponal and DI water followed by drying using compressed nitrogen air. At first silica nano-particles were coated on silicon wafer and then dried in air for about 2-4 min and then suncolloid nanoparticles were coated on the silicon wafer and dried in air for about 10-15 min, some samples were heat treated after suncolloid coating at around 80-90^{o}. The characterization was done using UV-Vis spectrophotometer, Ellipsometry and Scanning Electron Microscopy. The figure 1.10 shows the different snapshots taken during dip coating.

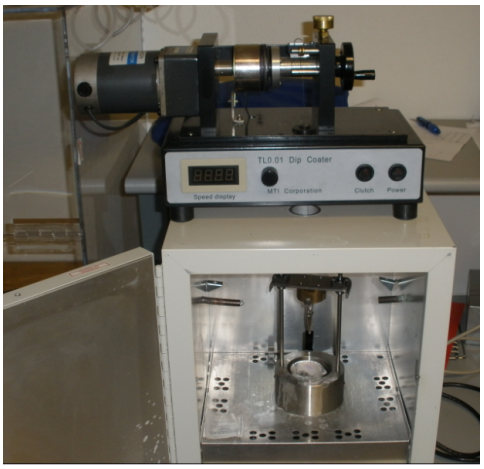

(a)

(b)

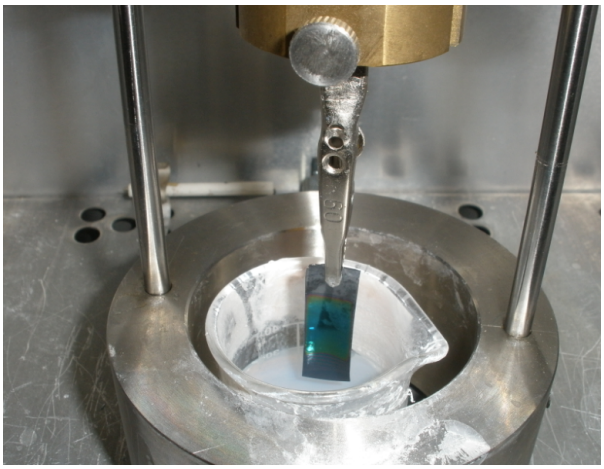

(c)

Figure 1.10 Dip coating set up (a) Immersion (b) Immersion for certain time and start up (c) withdrawal

1.2.2.3 Results and Discussions

A general study was done to know structural properties and reflectivity of the fabricated DBR. Two parameters, concentration and withdrawal speed were varied to know the effect. At first suncolloid solution was deposited at different concentrations and speeds to know the refractive index. Many numbers of samples were made by changing the concentration and speed to know the refractive index as shown in the table 1.1

Table 1.1: Measured Refractive index and thickness by ellipsometry

Concentration (wt %)	Thickness(nm)	Index	speed Display
7.64	72.23	1.5504	60
7.64	76.57	1.5535	80
7.64	67.76	1.5699	100
7.64	67.29	1.5606	140
1.91	24.09	15.6	60
1.91	24.51	14.68	80
1.91	22.6	13.92	100
1.91	23.14	14.69	120
1.91	18.34	14.62	140
15	191.9	1.47	60
15	150	1.48	140
15	178	1.52	240
20	239.4	1.52	60
20	170.4	1.49	100
20	200	1.5	140
20	258.7	1.58	240
25	248.2	1.76	60
25	240.8	1.57	100
25	287.8	1.72	140
25	381.2	1.64	240

From the table the values with red color are discarded as the refractive index was found to be very high. The refractive index was determined to be in the range of 1.5-1.57. A set of 6 samples were made to study the dip coating technique. The typical result for two samples one with heat treatment and another without heat treatment is discussed here. With a 15% of sun colloid and speed display of 80bits (Appendix A) and 7% of silica solution with speed display of 120 bits maximum peak obtained is 64.839% after 7 periods. After 8^{th} period the peak value decreased and shifted towards right and after 9^{th} period it further decreased and shifted to right as shown in figure 1.11.

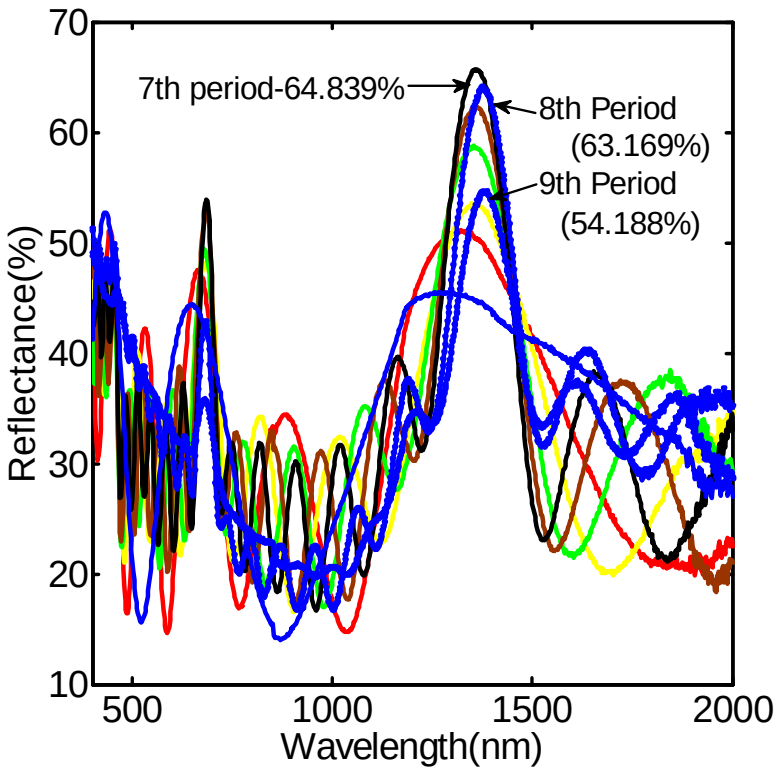

Figure 1.11 Measured reflection of heat treated dip coated DBR with silica and suncolloid nanoparticles

The corresponding cross section images of SEM are shown in figure 1.12.

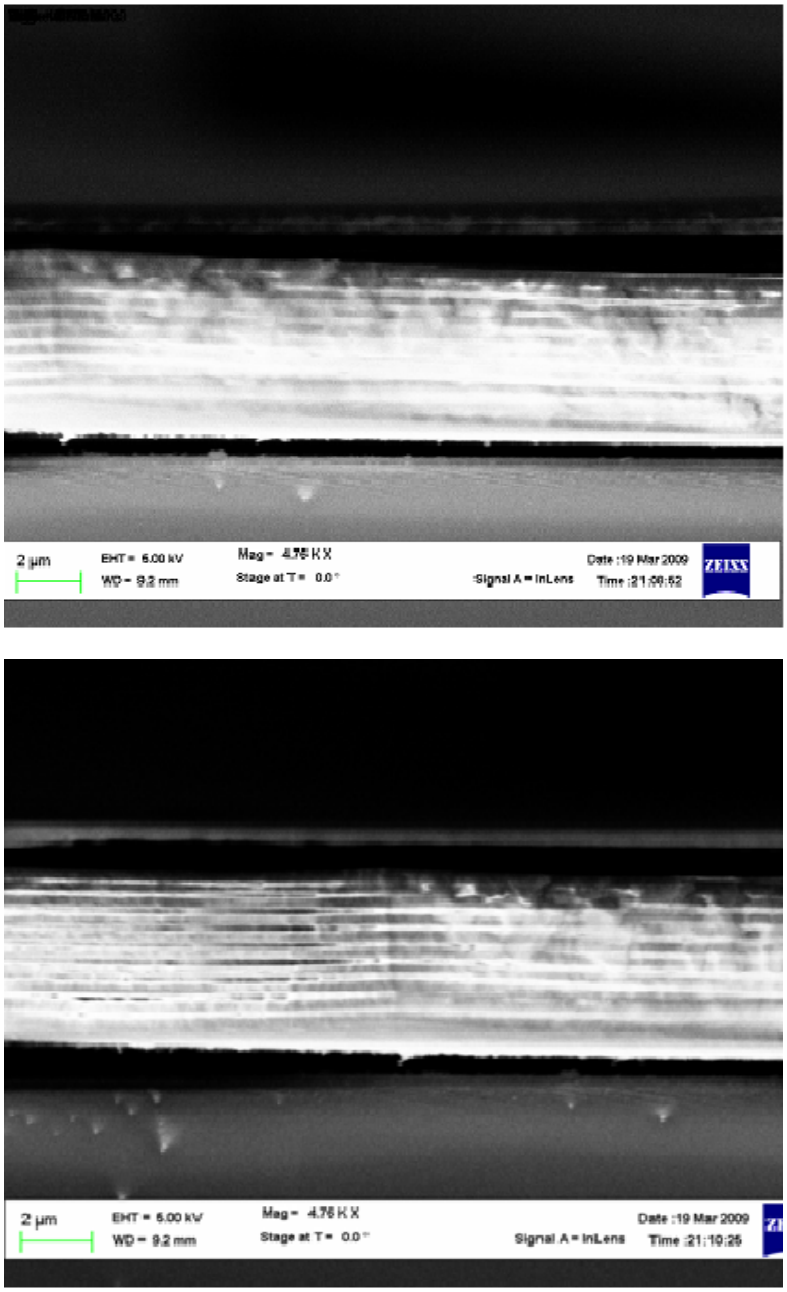

Figure 1.12 Cross section SEM images taken at two different places on the sample

Another sample at the same concentration and speed but without heat treatment was found maximum peak reflectivity value as 55.635% after 6 periods and it decreased to 42.815% of

reflectivity after 7th period as shown in figure 1.13 and cross section SEM images are shown in figure 1.14

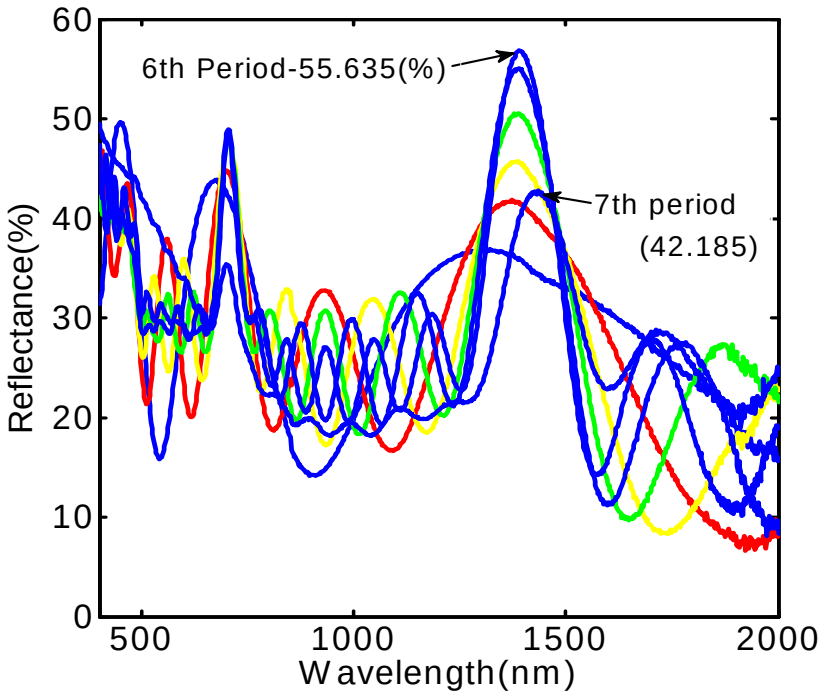

Figure 1.13 Measured reflection of non-heat treated dip coated DBR with silica and suncolloid nanoparticles

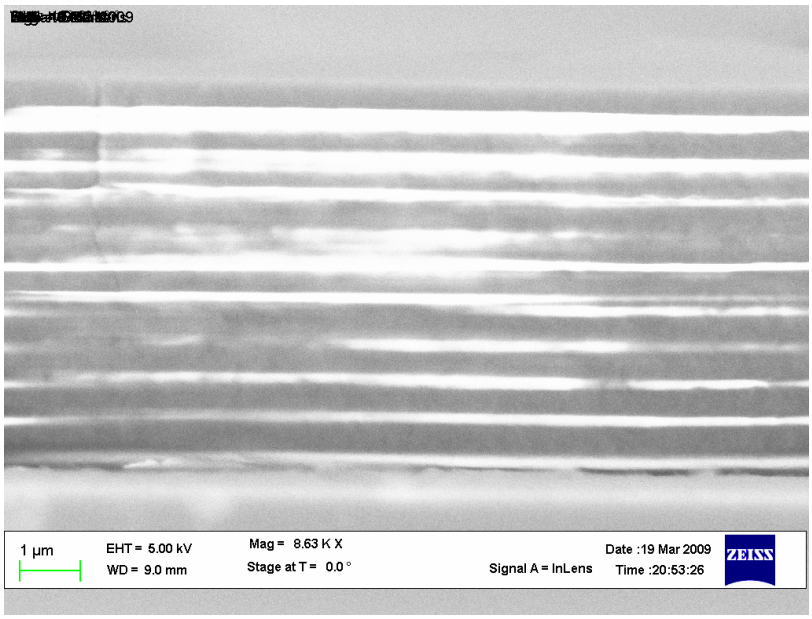

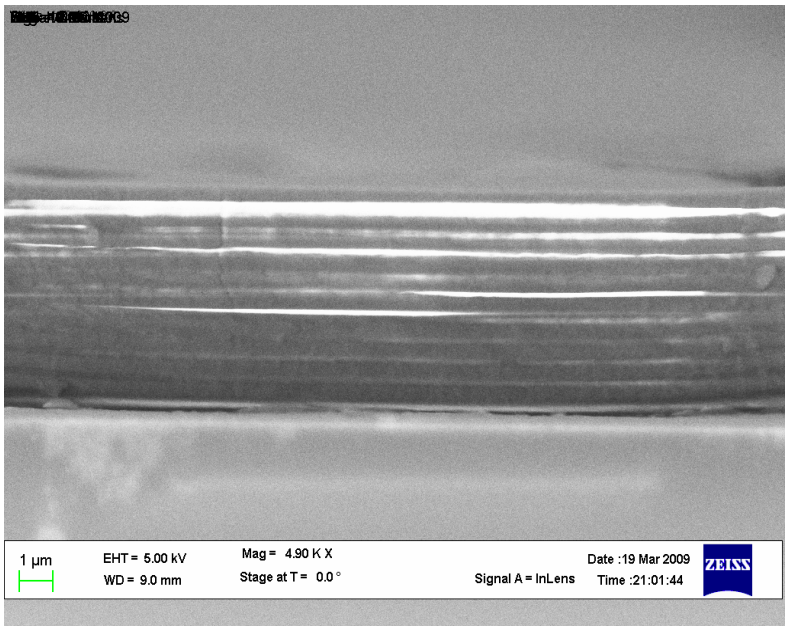

Figure 1.14 Cross section SEM images taken at two different places on the sample

On heat treated sample surface defects such as flakes, cracks and air gaps between layers can be seen from SEM image. After 7 periods of dip coating the peak reflectivity reduced, this could

be due to the thickness variation caused because of internal stress developed by the heating cycles. Regions of delamination can be seen at substrate and in between layers this could be due to the different thermal coefficient of the materials. Where as in non heat treated sample, thickness mismatching is found after depositing 4 or 5 periods this can be attributed to the presence of some wet films between layers leading to in sufficient bonding. In conclusion fabricated DBR structures were characterized to study the peak reflectivity and structural properties and more study to be done to know the effect of solvent, effect of withdrawal speed, effect of concentration, effect of substrate, effect of immersion time and effect of humidity to control the process.

CHAPTER 2

OMNI–DIRECTIONAL ANTI REFLECTION COATINGS ON AMORPHOUS SILICON SOLAR CELLS

The solution processed spherical texture is demonstrated on glass, quartz and on silicon substrates and it is found that it reduces the reflectivity in the wavelength regime of 400-1200nm[8]. This part of thesis is about the solution processed omni-directional anti-reflection (Omni-AR) coatings on commercial amorphous silicon solar cells. A monolayer of microscale spherical dielectric particles is first formed using convective coating method followed by a dielectric film with a film thickness that is fraction of the diameter of the particles. The spherical surface texture improved the efficiency at different incident angles at surface-normal (0^o), 30^o, 45^o and 60^o off-surface-normal. Current-Voltage characteristics showed the improvements in efficiency as high as 12% at different incident angles, demonstrating its omni-directionality. The experimental results were compared with the simulated results which agreed reasonably well[3]. The results obtained confirmed the solution-processed omni-directional anti reflection coating is a cost effective method particularly for commercially produced thin film amorphous silicon solar cells.

2.1 Theoretical background for antireflective (AR) silica coatings

The evaporation driven convective assembly can be used to fabricate anti-reflective (AR) coating on solar cells and other technologically relevant materials with controlled thickness and refractive index. An ideal homogenous antireflective (AR) coating achieves 0% reflection at a specific wavelength if the refractive index, n_c meets the condition $n_c = (n_a * n_s)^{1/2}$, where n_a and n_s are the refractive indices of air and the substrate respectively[9]. For example a glass

substrate (n_s =1.52) requires n_c of 1.23. Porous or microscopically layered dielectric materials can easily achieve an effective volume – averaged refractive index approaching 1.23 provided that the pore size is much smaller than the electromagnetic wavelengths of interest[10]. Silica sol-gel layers closely matching above relationship can provide good anti-reflection properties and are currently implemented in Antireflection film production. From the theory of AR coatings, Fresnel coefficient of reflection, r, for a thin film coating (of thickness 'l' and refractive index n_c) on a semi – infinite transparent substrate (n_s) is given by[9].

$$r = \frac{n_c(n_a - n_s)\cos kl - i(n_s - n_c^{\,2})\sin kl}{n_c(n_a + n_s)\cos kl - i(n_s + n_c^{\,2})\sin kl} \qquad (2.1)$$

Where the ambient medium is usually air, n_a = 1, k is the reciprocal space wave number, $k = 2\pi / \lambda n_c$ and λ is the wavelength of light. The actual reflectance, R, of the coating/substrate is same as $|r|^2$. The light reflected from the surface of the substrate and from the surface of coating destructively interfere with each other to achieve complete transmission or zero reflection when thickness of the coating is equal to the quarter wavelength of the incident light ($kl = \pi / 2$). The reflectance 'R' for a quarter wave coating of such thickness ($l_{1/4} = 0.25\lambda / n_c$) simplifies to:

$$R = \frac{(n_s - n_c^{\,2})^2}{(n_s + n_c^{\,2})^2}$$

From the equation mentioned above $n_c = (n_a * n_c)^{1/2}$, refractive index of air n_a = 1 and R becomes 0, when $n_c = n_s^{\,1/2}$.

2.2 Current-Voltage Characteristics of a Solar Cell

The typical current- voltage characteristics of a solar cell under illumination are shown in figure 2.1. The energy conversion efficiency of a solar cell is defined as the generated output electrical power to the incident optical power under standard test conditions (25^{o}C, AM1.5), i.e., $\eta = \frac{P_{\max}}{E \times A} \times 100\%$, where η is the percentage in efficiency, $P_{\max}$ is the maximum Power Point $(I_p \times V_p)$ (Figure2.1), E is the input light irradiance in W/m2 , A is the area of the solar cell in m2 .

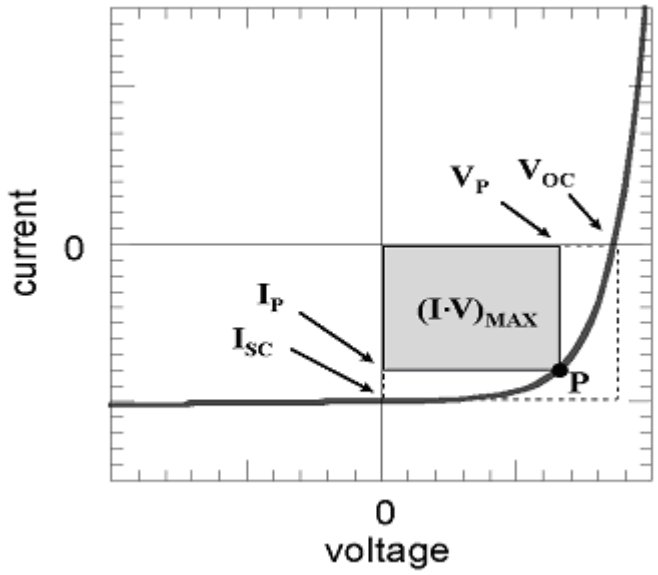

Figure 2.1 I-V curve of a typical solar cell (I_{sc} = Short Circuit Current, V_{oc} = Open Circuit Voltage, $(I.V)_{MAX}$ = Maximum Power Point)

2.2.1 Open Circuit Voltage (V_{oc})

Open circuit voltage is the difference in electrical potential between two terminals of the device when there is no external load i.e., theoretically under infinite resistance; in this cases the circuit is open up. So, the solar cell under this condition there is no external current produced.

2.2.2 Short Circuit Current (I_{sc})

Short circuit current is the current through the solar cell when voltage across the solar cell is zero, i.e., theoretically under zero resistance, usually it is the current obtained when two opposite terminals of the cell are connected. Ideally for a solar cell under minimum resistive loss mechanisms short circuit current and light generated current are equal.

2.2.3 Maximum Power Point (P_{max})

It is the point on the current –voltage curve under illumination, where the product of current and voltage is at its maximum. The corresponding point on current axis is I_p (current at maximum power) and V_p (voltage at maximum power).

$$P_{\max} = I_p \times V_p$$

2.2.4 Fill Factor (FF)

FF is the ratio of maximum power from the solar cell to the product of Voc and Isc. Graphically it is the measure of squareness of the solar cell or it is the area of largest rectangle which will fit in the current –voltage curve

$$FF = \frac{P\max}{I_{sc} \times V_{oc}} = \frac{I_p \times V_p}{I_{sc} \times V_{oc}}$$

So energy conversion efficiency can be written as, $\eta = \frac{FF \times I_{sc} \times V_{oc}}{E \times A}$

2.2.5 Quantum Efficiency

Quantum Efficiency is the ratio of the number of carriers collected to the number of photons of a given energy incident on the solar cell. External quantum efficiency (EQE) includes the effect of optical losses i.e., it is the fraction of photons that are converted to electrical current. Internal quantum efficiency (IQE) refers to the fraction of photons (not reflected or transmitted out of the cell) that are converted to electrical current. $EQE = IQE \times (1 - R - T)$

2.3 Experimental Apparatus and Techniques

The suspension of monodispersed 2µm silica microspheres were used as purchased from Microspheres-Nanospheres, a Corpuscular company. The figure 2.2 shows the photograph of a bottle containing Silica microspheres and spin-on-glass (SOG)

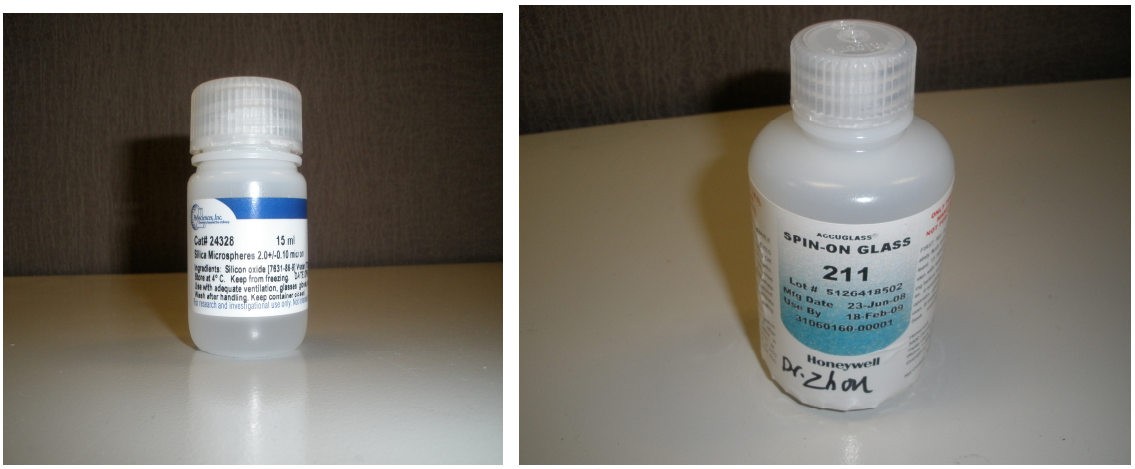

(a) (b)

Figure 2.2 Bottle containing (a) 2µm silica microspheres (b) spin on glass.

The spin-on-glass (SOG), Accuglass^{R} 211, with a specified thickness of 0.22µm, was used as purchased from Honeywell (figure1). SOG is a dielectric material usually SiO2 doped with phosphorous or boron and is suspended in a solvent solution. It is used here because of same refractive index that of silica microspheres, to fill the gaps between microspheres and act as a glue, to planarize and form hemispherical structure. Commercial amorphous Silicon Solar cells were used in the experiments which are bought from PowerFilm® S3-37 with a size of 64×37 mm^2. The commercial amorphous Silicon Solar Cells came encapsulated with plastic cover. The plastic cover was removed and stacked on a glass slide using double sided tape to make the cell flat, so that it is convenient to deposit monolayer silica microspheres and SOG. The PowerFilm® amorphous Silicon solar cell is a thin, flexible fabricated on a polyimide substrate as thin as 0.025mm. It consists of 5 cells in series with a total voltage of 5volts and two copper

leads as positive and negative terminal at each end as in the figure 2.3 . The amount of silicon used by the PowerFilm® to produce amorphous Silicon solar cell is as low as 1% of the amount used in traditional crystalline silicon solar cells.

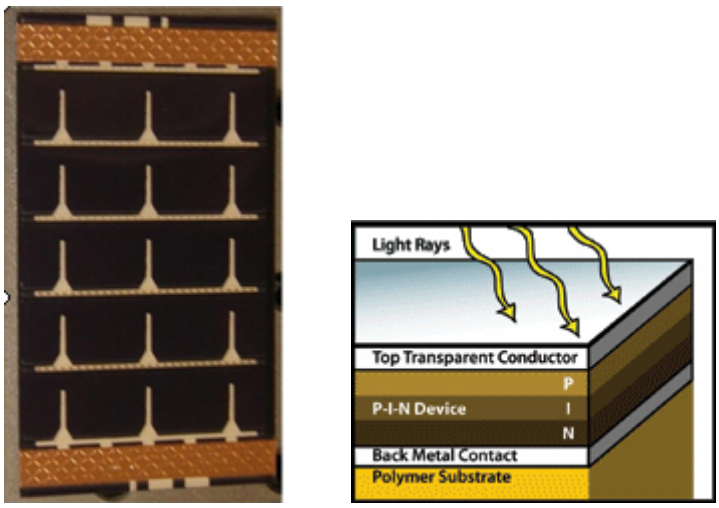

(a) (b)

Figure 2.3 (a) Photograph of a PowerFilm® Amorphous Silicon Solar cell (b) Cross sectional view of the PowerFilm® Amorphous Silicon Solar cell

2.3.1 Convective Assembly and Monolayer formation

The convective assembly set up used is similar to that of Prevo and Velev[4]. The typical convective assembly used for coating the amorphous silicon solar cell is as follows. A controlled amount of silica microspheres suspension was injected into the wedge (~25^{o}) formed between amorphous silicon solar cell and the coating plate and is entrapped there by capillarity as shown in figure 2.4. The coating plate speed ranging from 0.01-0.25mm/sec is programmed thus the liquid meniscus is dragged horizontally across the substrate. The various coating parameters like coating plate speed, dispersed suspension volume, wedge angle and solvent (ethanol and water) are tried to get a close packed monolayer of particles. Monolayer formation was able to obtain at coating plate speed of 0.17-0.20 mm/s, suspension volume of 60-65µl and ethanol as solvent rather than water because of quick evaporation of ethanol. The microsphere concentration also varied in between 5-16% where at 7-9% concentration close packed

monolayer was formed. The parameters mentioned above are dependent on each other. By changing any one parameter resulted in loosely packed or multilayer formation. The wedge angle was fixed at around 25^{o} and the plate speed and dispersed suspension volume were varied to obtain a closely packed monolayer shown in figure 2.4.

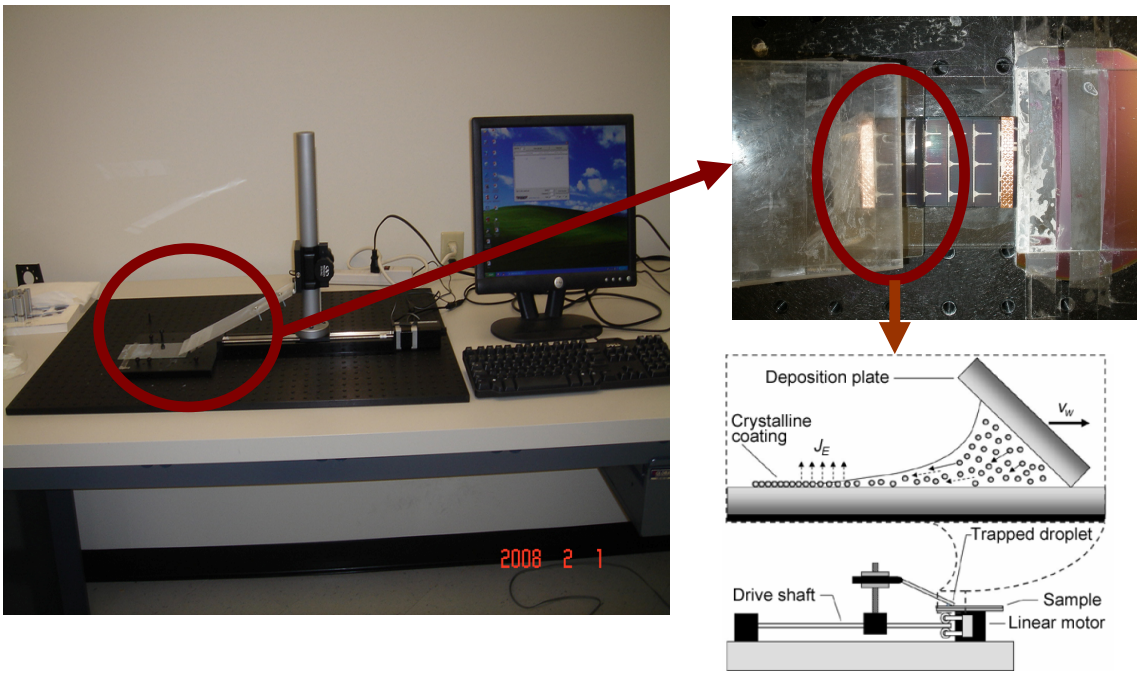

(a) (b)

Figure 2.4 (a) convective assembly set up (b) schematic of particle coating and drive motor

2.3.2 Omni-AR coating

After the formation of uniform and closely packed monolayer, SOG is spin coated onto to the solar cell at 1000rpm for 30 sec and then heated on a hot plate at 90^{o}C for 1-2 min to remove solvent and to cross link the SOG film.

2.3.3 Coating Characterization

Coating reflectivity of normally incident light was measured using a UV/VIS spectrophotometer (JASCO V-570, Jaso Corp., Japan) over the spectral range of 400-1200 nm. The microstructure of omni–AR coatings is studied with a Zeiss SUPRA 55 VP scanning electron microscope (SEM). The surface roughness on solar cells before omni-AR was measured by profilometry (Alpha Step IQ surface profiler). I-V characterization before and after omni-AR coatings was done using 100W quartz tungsten halogen (QTH) light source (Newport Oriel 6333). The home made angle dependency set up was used to measure I-V characteristics at different incidence angles. A mirror is used which reflects the incident light onto the solar cell. By moving and rotating the mirror, the incident angle on the solar cell can be controlled from 0^o to 60^o as shown in the figure 2.5. The electrical response is measured using source-measuring unit (SMU) called source meter. Keithley 2601 is used as a source meter. Typical voltage ranges set for the above mentioned solar cell are -5V to +5V. It is possible to perform two point contact and four point contact probes; here four point contact probes are used in order to reduce the contact/serial resistance.

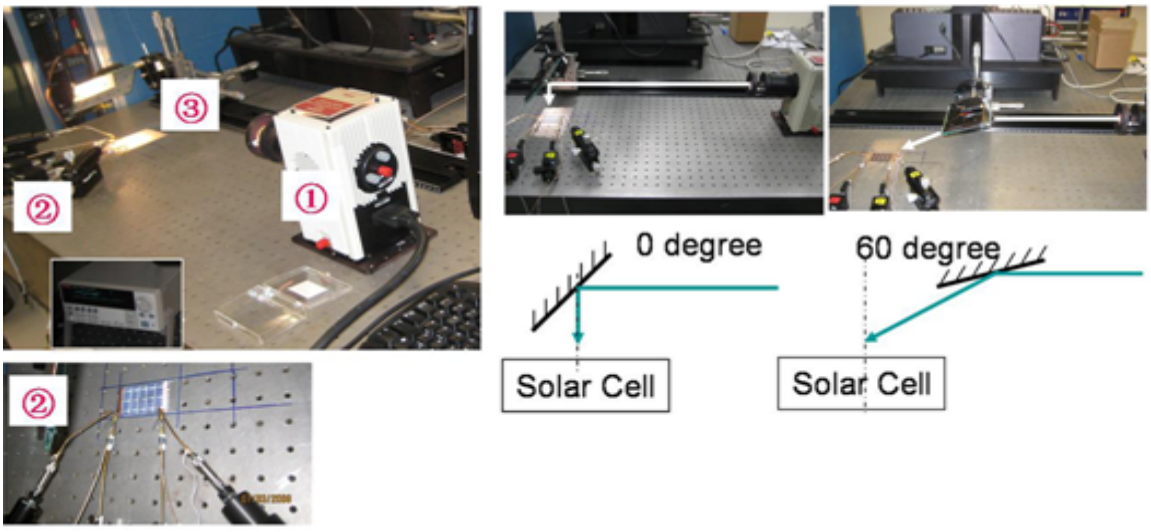

Figure 2.5 Experimental setup for angle dependent current-voltage measurements. Incident angles of 0^o and 60^o are shown as examples (1) 100W QTH lamp (Newport Oriel 6333) (2) Four probe with Keithley 2601 source meter (3) Angle-control mirror stage

2.4 Optical Design and Simulation

Theoretical investigation has been done on omni-AR coatings for amorphous silicon solar cell to verify the performance. After silica microspheres deposition, SOG, a dielectric film having same refractive index to that of microspheres is spin coated to obtain hemispherical shape. SEM images of omni-AR coatings clearly shows close match to the hemispherical particle shape with a 0.2µm SOG film as shown in figure 2.6.

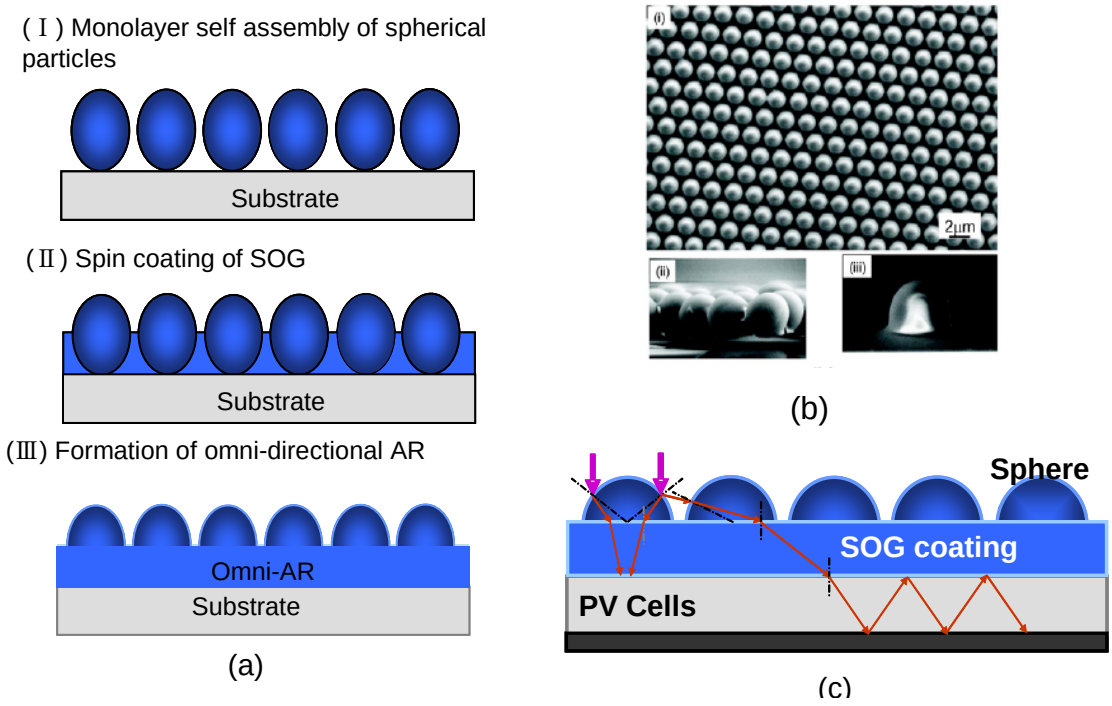

Figure 2.6 (a) Omni-AR coating based on monolayer of spherical particles and SOG film (b) SEM images of fabricated omni-AR coatings (i) top view (ii) cross sectional view before SOG film (iii) cross sectional view after SOG film (c) schematic representation of normal incident light entering the Photovoltaic cell [2]

The geometric structure under consideration is shown in figure 2.7. The structural parameters considered are mentioned in the Table 2.1. The dispersion curves for refractive index and extinction coefficient of amorphous silicon are shown in figure 2.8.

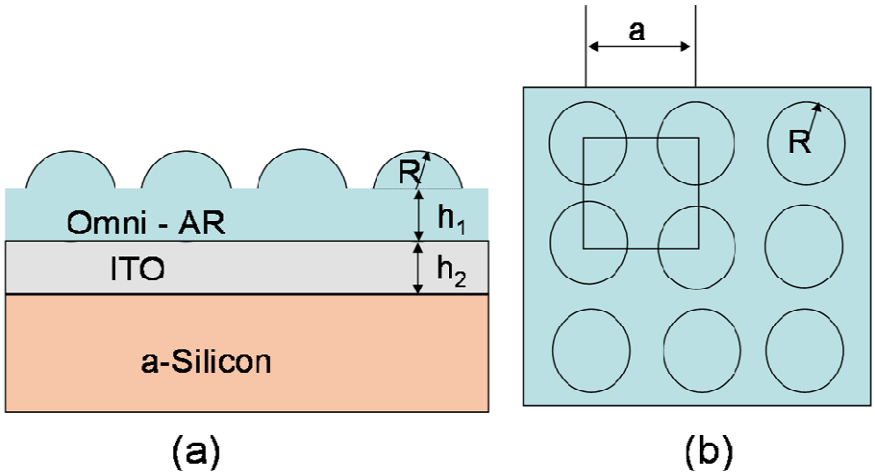

Figure 2.7 The hemispherical grating structure as the basic anti reflection structure for simulation (a) cross section view (b) top view

Table 2.1 The parameters considered for simulation of omni-AR structure

Parameters	(µm)
Thickness of SOG film (h1)	0.2
Thickness of ITO (h2)	0.05
Radius of Microspheres, R	1
Period (a)	2.5
Refractive Index of SiO2 and SOG	1.46
Refractive Index of ITO	1.8

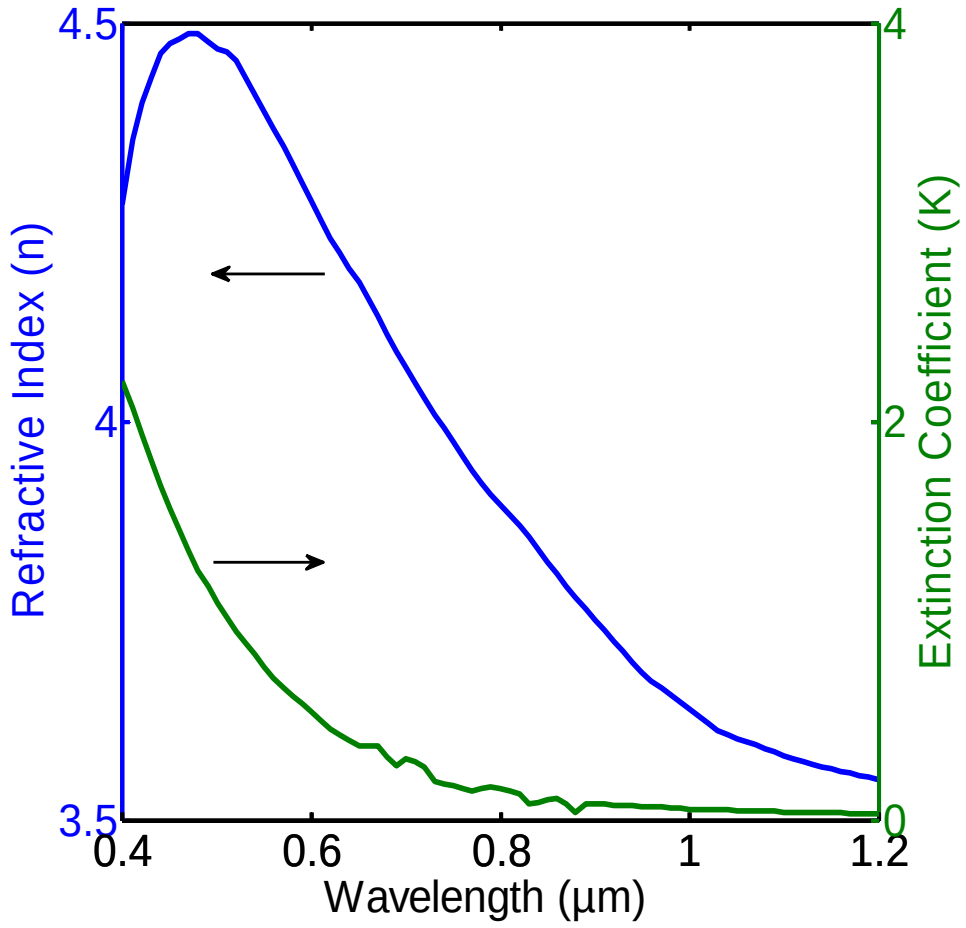

Figure 2.8 Dispersion curve of amorphous silicon representing refractive index (n) and extinction coefficient (k) [27]

The complex refractive index is expressed as **n**=n+ik, where n and k are real and imaginary part of refractive index, respectively. The imaginary part k, the extinction coefficient is linked with absorption coefficient by the relation, $\alpha = 4\pi k / \lambda$ where λ is the free–space wavelength. The simulation is based on rigorous coupled wave analysis[2], which analyzes the diffraction of an electro-magnetic plane wave incident obliquely on a lossless grating structure composed of materials with different refractive indices. Reflectivity (R [λ, θ]) is calculated at different angles (0^o, 30^o, 45^o, 60^o) using transfer matrix method and coupled diffraction method. The reflectivity calculations are done with omni-AR coating and without omni-AR coating. Quartz

Tungsten Halogen (QTH) Liquid Guide calibrated spectra is used as light source to calculate incident photon flux which is also a spectral dependent. With the simulated spectral dependent reflection data, the total absorbed photons are calculated. Here the intensity of spectra incident on the sample is assumed constant and only the reflectivity impact is accounted. The generated electron hole pair is calculated based on the wavelength dependent internal quantum efficiency of amorphous silicon (figure 2.9) and number of photons absorbed. Assuming the open circuit voltage and fill factor as constant, short circuit current density for with and without omni-AR and efficiency enhancement is calculated as described in the figure 2.10.

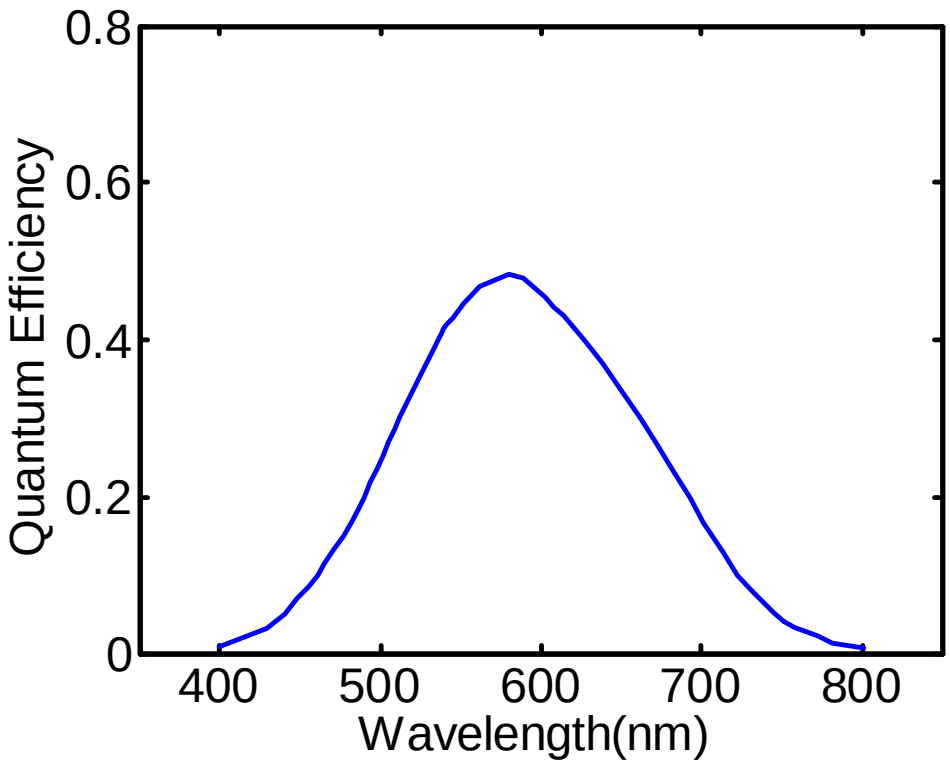

Figure 2.9 Internal Quantum Efficiency of Amorphous Silicon [27]

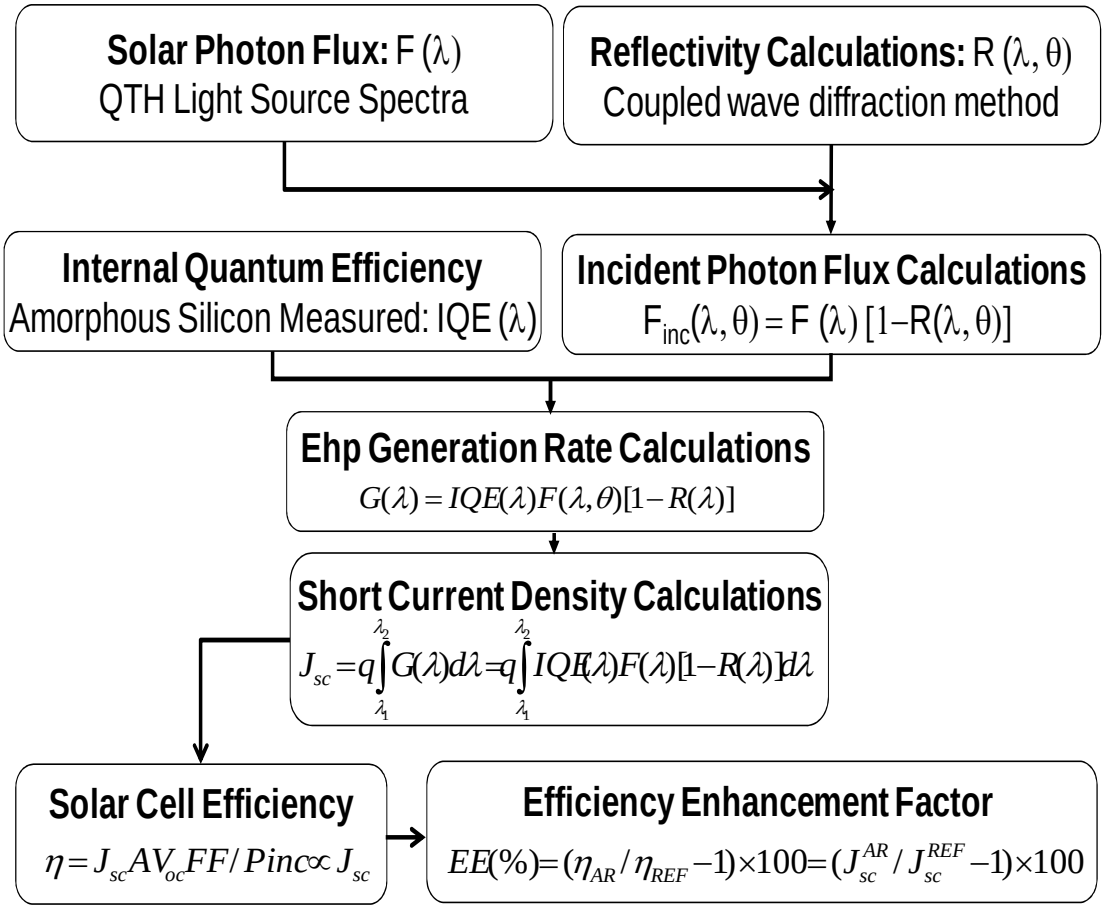

Figure 2.10 Reflection impact simulation procedure for solar cell performance evaluation

2.5 Results and Discussion

The electrical, optical and structural characteristics are discussed in this section. Experimental results for reflectivity for with and without omni – AR coatings and solar cell output electrical parameters and efficiency enhancements for many numbers of samples were statistically analyzed. Finally these results were compared with the simulated results and verified the performed of solar cell.

2.5.1 Structural characterization of Omni-AR coatings

The amorphous silicon solar cell is encapsulated in a plastic cover. This plastic cover was removed and the surface morphology was studied using SEM and Alpha step profiler. The surface of solar cell consists of ITO and two copper leads as negative and positive electrodes at each end. The morphology of ITO is neither smooth nor dense rather it has porous structure with small interconnected grains as shown in figure 2.11

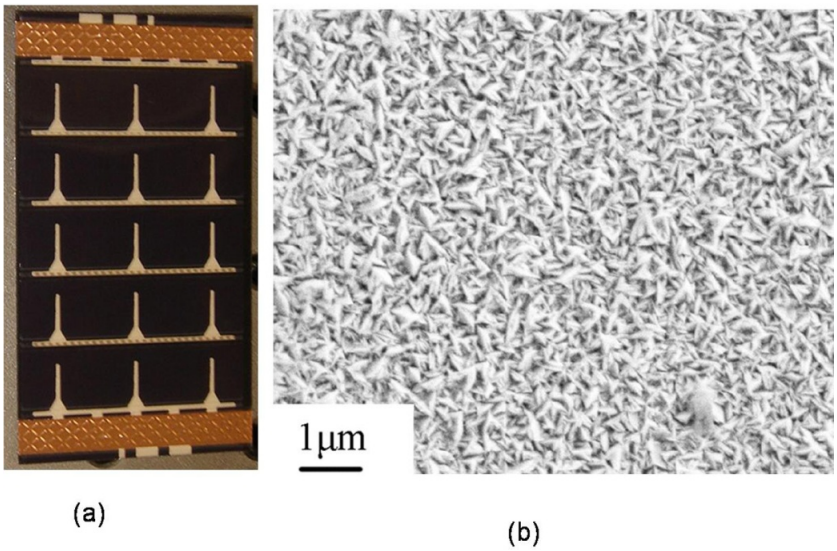

Figure 2.11 (a) Photograph of a PowerFilm amorphous Silicon solar cell and (b) SEM image of the surface morphology of the cell after removal of the plastic cover

The surface roughness is in the range of 0.2-0.3µm. The height of copper leads above the ITO film is around 8-10µm. The presence rough surface is a challenge to the formation mono layers of silica particles over the entire surface of the cell. The convective assembly offers a fine control over the coating properties by the controlling the coating plate speed which allows sufficient time to deposit. Uniform and closely packed monolayer were able obtain with coating plate speed at around 0.18mm/s as shown in figure 2.12.

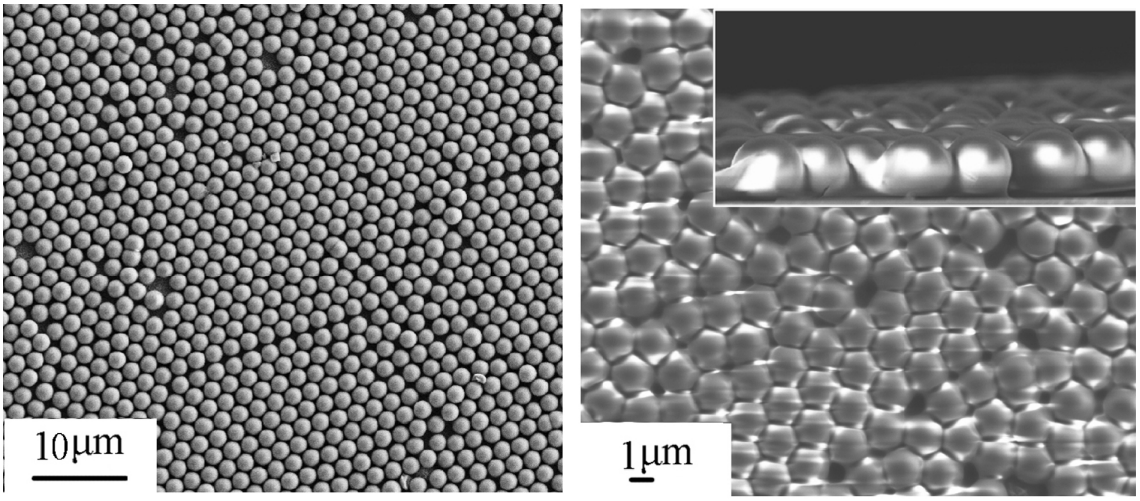

Figure 2.12 (a) SEM image of a solar cell coated with a monolayer of 2-μm silica microspheres and (b) followed with a 0.2-μm SOG 211 film. The insert in (b) is a side view of the omni-AR structure

More multi layers and submonolayers with voids formed at some regions, which are attributed to the non-uniform distribution of silica microspheres at the meniscus during coating and rough structure of the surface. Most of the region is closely packed structure with close resemblance to hexagonal structure. The packing density is improved and microspheres are held together by SOG film as shown in figure 2.12 (b)

2.5.2 Optical Characterization of Omni-AR coatings

The normal incidence reflectivity for with Omni-AR coating, SOG film only, without omni-AR and microspheres was measured over the spectral range of 400-1200nm using UV/Vis spectrophotometer as shown in figure 2.13. From the figure 2.13 we can see the reflection reduces with omni-AR coatings considerably, where as there is a little change in reflectivity when compared coating with SOG only and without coating. The reflectivity increased on coating with microspheres only, this is due to multiple surfaces in the spherical micro particle and the surface of the solar cell. According to the theory and simulated results the top surface of the coated particle should be narrow and the interface between substrate and particle should be

broad[2]. Therefore the hemispherical structure accomplishes reduction in reflection, which is obtained by SOG film. So, SOG film not only acts as glue between microspheres to hold together but also reduces number of surfaces which increases reflection.

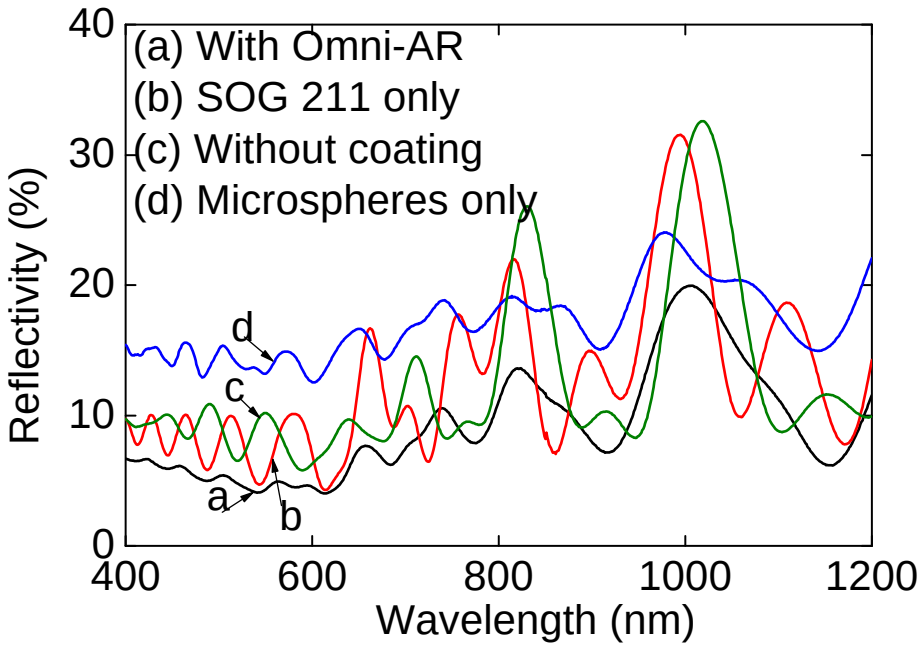

Figure 2.13 Measured surface-normal reflectance of amorphous silicon solar cells (a) without coating, (b) with SOG 211 only, (c) with monolayer silica microspheres only, and (d) with the omni-AR structure

The above analysis shows that the hemispherical structure reduces the reflectivity, in order to verify these results computer simulations were carried out for the mentioned structure in the optical design section along with key parameters. In order to fit the experimental results ITO thickness is adjusted during simulation, and found best fit at thickness of 50nm as shown in figure 2.14(a).

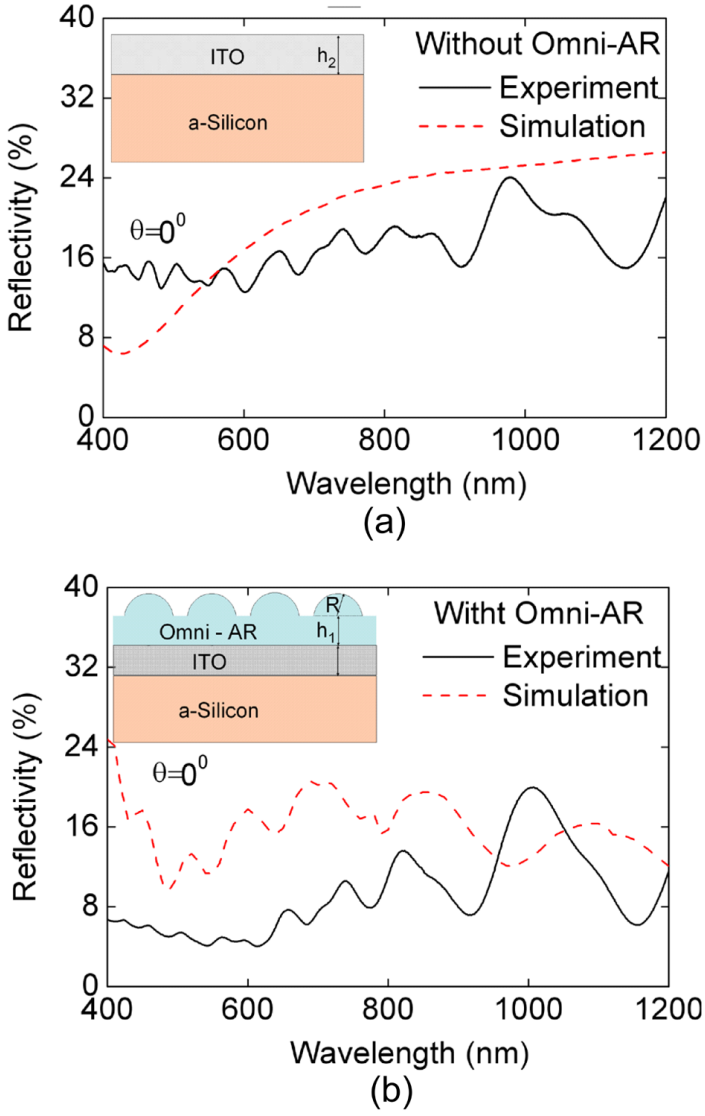

Figure 2.14 The measured and simulated reflectivity for amorphous silicon solar cells (a) without and (b) with Omni-AR coatings under surface- normal incident conditions

The difference in measured and simulated reflectivity is due to the ITO thin film. From the figure 2.11 the surface morphology is not smooth, with small interconnected grains. But the surface of ITO is assumed as ideal and smooth in the simulations. With these considerations a reasonably good agreement with measured values was able to achieve as shown in figure 2.14(b).The simulated reflectivity at different incident angles such as 30^o, 45^o, and 60^o were carried out. It

was observed that significant reduction in reflection is achieved at larger angles, thus indicating omni directionality as shown in figure 2.15.

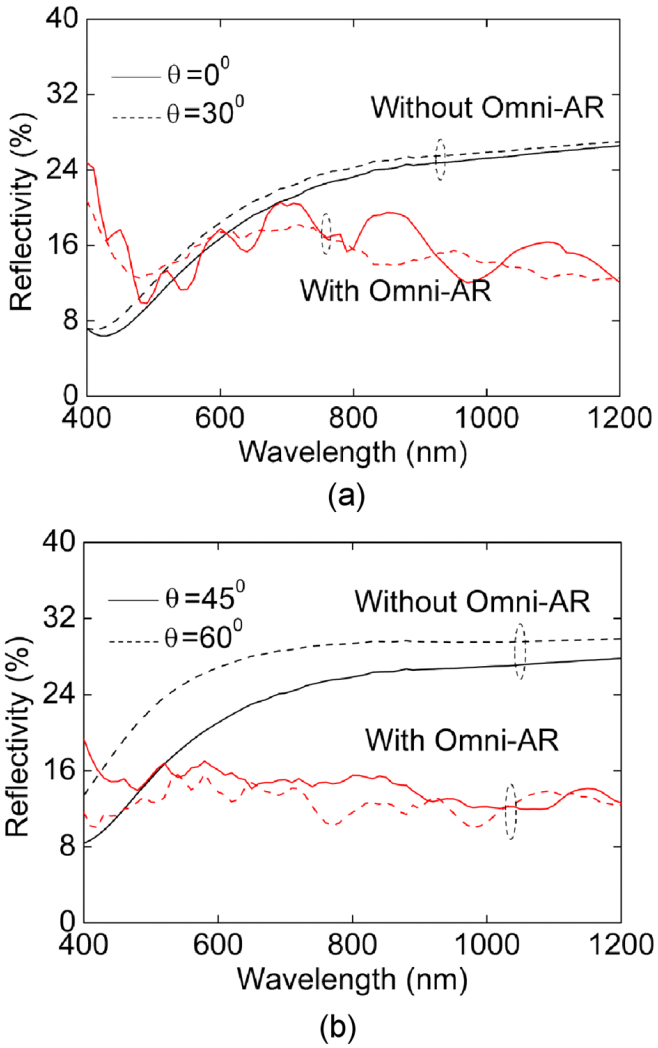

Figure 2.15 Simulated reflectivity of amorphous silicon solar cells without and with omni-AR structure at (a) small incident angles (θ=0° and 30°) and (b) large incident angles (θ=45° and 60°)

2.5.3 Electrical Characterization of Omni-AR coatings

Current – Voltage characterization was carried out to get output electrical properties of the solar cell for with and without omni AR coating, which ultimately evaluates the performance. An angle dependent measurement setup was built using a mirror which can rotate and reflects the light on to the solar cell as shown in figure 2.5. Many numbers of solar cells were tested and

out of which a set of eight solar cells were tested to minimize any statistical variation associated with the test set up. A typical current–voltage characteristics of a solar cell measured at different incidence angles of light is shown in figure 2.16.

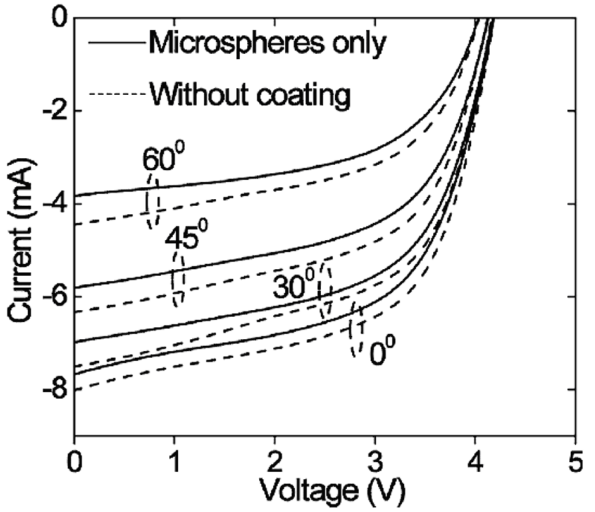

(a)

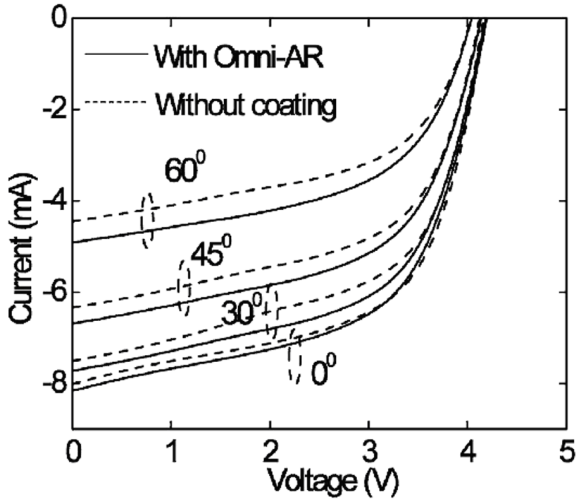

(b)

Figure 2.16 (a) Measured I-V characteristics of amorphous silicon solar cells without coating and with monolayer silica microsphere coating only and (b) without coating and with the omni-AR coating structure

From the current-voltage curves it is evident that with only microspheres coating the open circuit voltage (V_{oc}) remained almost unchanged but the short circuit current (I_{sc}) reduced for the entire

incident angles measured, which ultimately indicates there is reduction in efficiency. This proves the analysis concluded from optical characteristics section, where multiple surfaces of the microspheres reduce the absorption of optical power, as a result of increased reflection (figure 2.13). Where as, shown in figure 2.16(b), short circuit current increased with omni-AR coating, for all incident angles measured. These results agree very well with the simulated reflection results at different incident angles (figure 2.15). Thus demonstrates the omni directionality for wide spectral range with the omni-AR coatings. It is interesting to note that the improvement in efficiency is greater at large angle of incidence. The photovoltaic parameters, I_{sc}, V_{oc} and P_{max} as a function of incident angles are shown in figure 2.17.

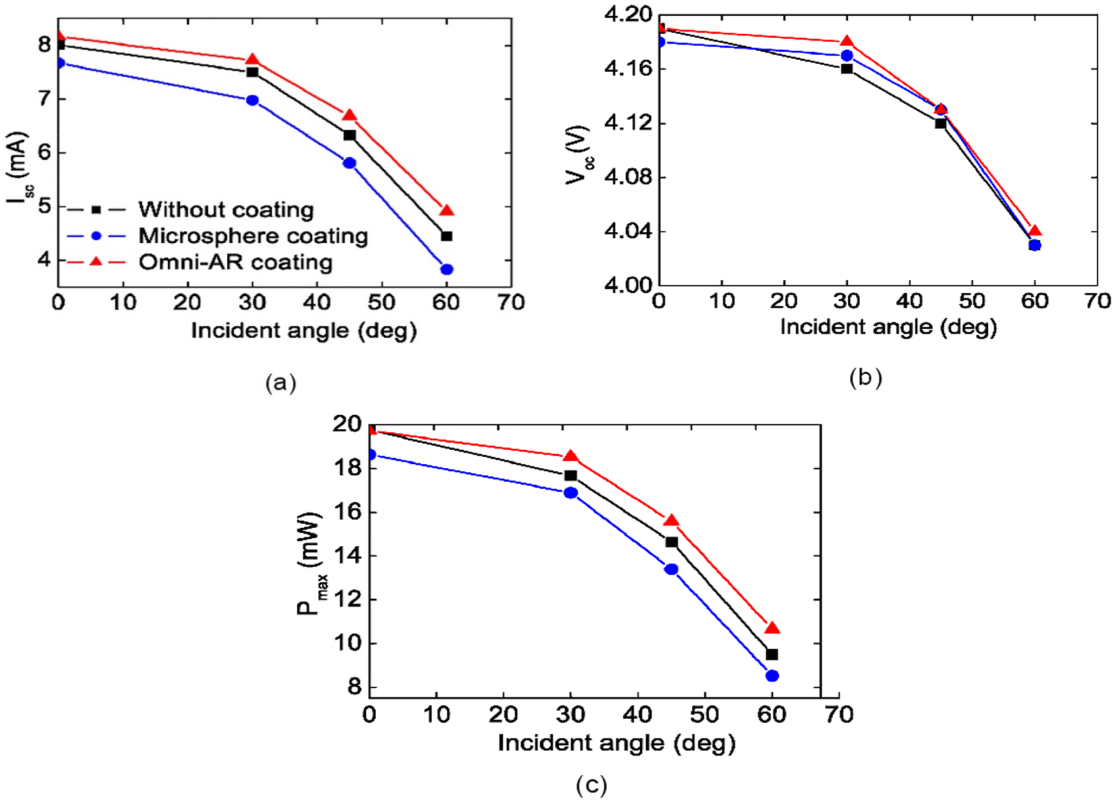

Figure 2.17 Photovoltaic parameters, as a function of incident angle for amorphous silicon solar cells without coating, with monolayer silica microspheres only and with the omni-AR structure. (a)I_{sc} (b) V_{oc} and (c) P_{max}

The improvement in P_{max} with the omni–AR coatings comes mainly from larger I_{sc}, while V_{oc} exhibits little change with both omni-AR coatings and coatings with only silica microspheres. This indicates due to enhanced light coupling into the solar cell by the omni-AR coatings is inherent reason for increase in P_{max}. The relative efficiency enhancement for the solar cell with microspheres only, SOG only and with omni-AR was calculated as shown in figure 2.18 and the maximum efficiency enhancement was found to be 12% at 60^{o} of light incidence.

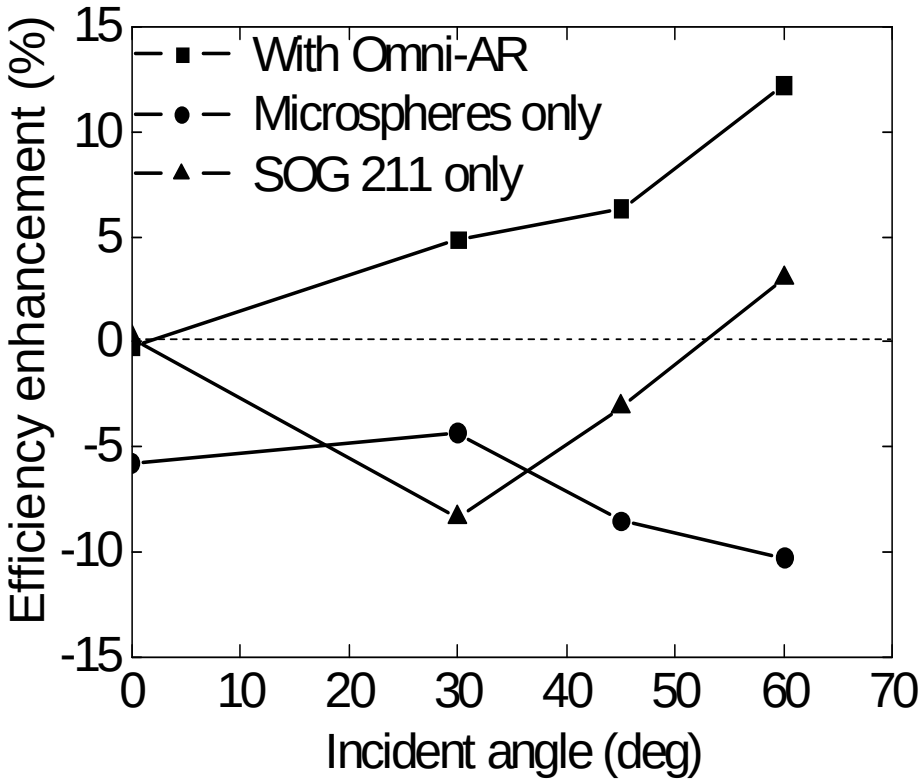

Figure 2.18 Relative enhancement in efficiency as a function of incident angle for amorphous Si cell with the omni-AR structure, with monolayer silica microspheres only and with SOG 211 only

The relative efficiency enhancement for the set of eight solar cells was calculated as shown in figure 2.19; the square symbol indicates the mean value. It shows that statistically the improvement in efficiency enhancement is feasible.

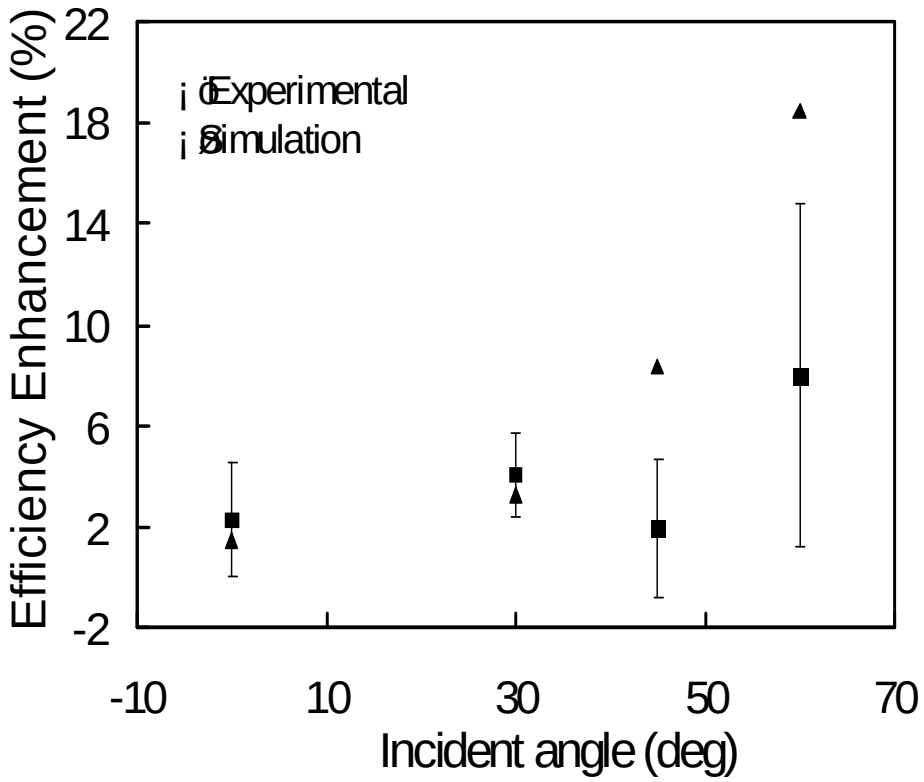

Figure 2.19 Statistics of relative enhancement in efficiency as a function of incident angle for eight amorphous silicon solar cells with the omni-AR structure. It also shows the simulated relative enhancement in efficiency with the omni-AR structure

CHAPTER 3

OMNI – DIRECTIONAL ANTI REFLECTION COATING ON ORGANIC SOLAR CELLS

In this chapter the practicability of solution processed omni directional anti reflection coatings has been demonstrated on organic solar cells. The organic or polymer solar cells are made by solution processing of polymers which is a very inexpensive process compared to fabrication of silicon solar cells. The typical device structure used to fabricate organic solar cell is shown in figure 3.1

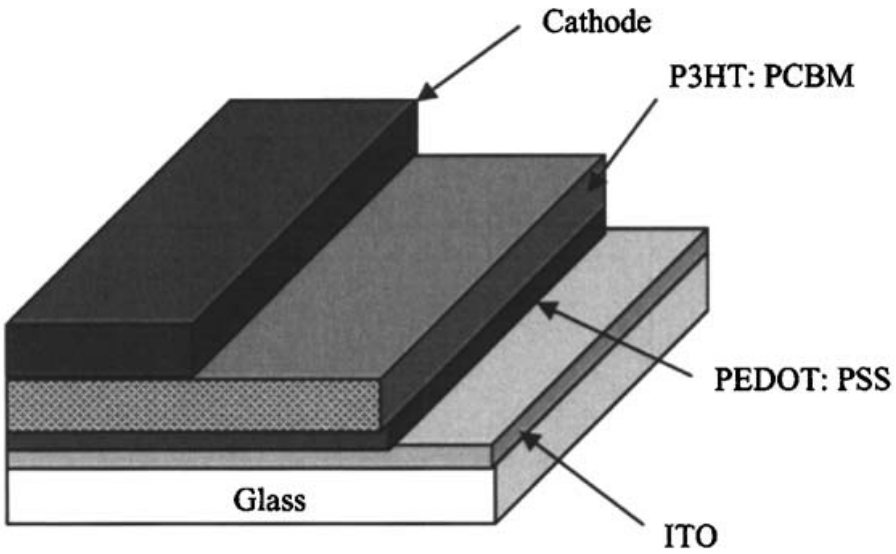

Figure 3.1 Organic solar cell structure with blend P3HT: PCBM as active layers and PEDOT: PSS as hole conducting semiconductor and aluminum as cathode [23]

The present organic solar cells fabrication is based on bulk heterojuction concept[25] i.e. donor material (polymeric material) is mixed with an acceptor (a soluble fullerene) in an organic solvent and then spin coated on a substrate of indium tin oxide (ITO) on glass followed by

annealing. During annealing, a micro phase separation takes place by the formation of an interpenetrating network and finally aluminum as the cathode (metal electrode) is evaporated on to the top. Excitons are generated on light absorption and are short-lived due to very poor charge carrier mobility generally with a diffusion length in the order of 10nm. However their strong absorption coefficients (>10^5 cm^{-1}) partly balances the low mobilities, giving high absorption in even diffusion length ~100nm range[24, 25]. The band gap of a polymer is critical in the absorption of light. Band gap of polymer is defined as the difference between the highest occupied molecular orbital (HOMO) and the lowest unoccupied molecular orbital (LUMO). The schematic representation of band gaps for individual layers is shown in figure 3.2.

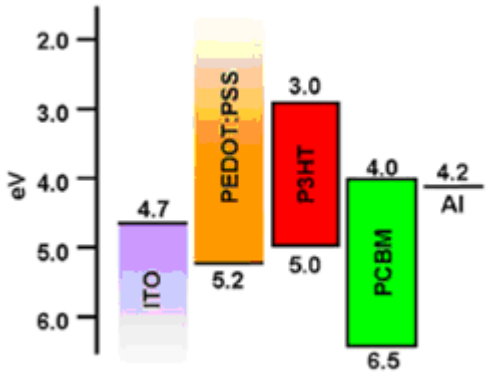

Figure 3.2 Energy level diagrams of device components of organic solar cell referenced to vacuum level [26]

PEDOT: PSS (Poly (3, 4-ethylenedioxythiophene) poly (styrenesulfonate)) which is a hole acceptor and which is spin coated first on ITO-glass substrate should have sufficient optical transparency to allow solar spectrum entry to the active layer requiring a wide band gap (>3ev). It should also be effective in blocking electron access while efficiently transporting holes to the anode (ITO). P3HT (poly 3-hexylthiophene) which is an electron donor has an absorption that extends up to 650nm. Typically low band gap polymers have better absorption spectra that extend above 600nm. The reason is at low band gaps more number of photons can be absorbed thus broader spectra can be utilized. There is also some optical loss when passing

through ITO-glass substrate. Therefore, because of stack of 3-4 thin layers in an organic solar cell, there is always certain percentage of light lost by reflection at the interfaces and absorption in layers other than the active layer. One of the potential possibilities to optimize the usage of incident light on organic solar cell without changing morphology of the device is the application of anti reflection coatings.

3.1 Omni-AR Coating

The same convective assembly and principle was used to coat omni AR on ITO-glass substrate with only some coating parameters variation. The ITO coated glass substrate was used as purchased from Nanocs^{R}. The total thickness of ITO-glass substrate is 1.1mm and ITO thickness accounts to 50-100nm with 50 ohm/square as surface resistance.

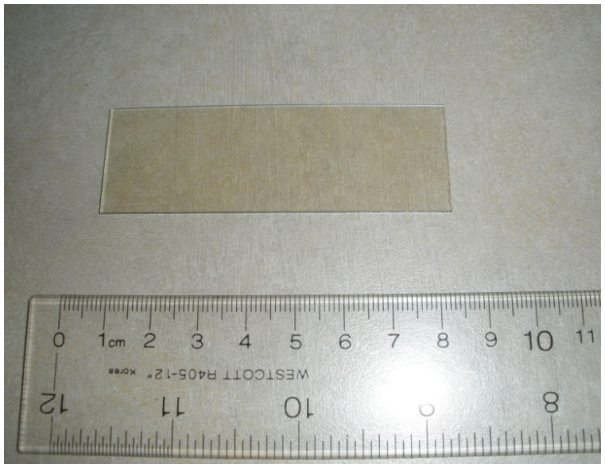

Figure 3.3 ITO –coated glass substrate beside the scale

The ITO-glass substrate was masked with an ordinary tape and non-masked area was etched with hydrochloric acid (49% w/v) for about 10 min as shown in figure 3.4

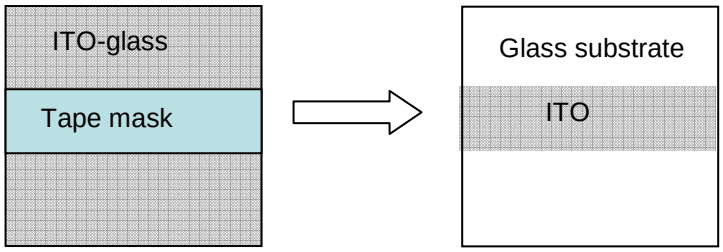

Figure 3.4 Schematic top view of (a) tape masked ITO-glass and (b) HCl etched ITO-glass

The etched substrate was cleaned with acetone, iso-proponal and DI water in an ultra sonicator to remove any particles and adherents and dried using compressed nitrogen dry air. Two micron spherical silica particles were coated on the glass side of ITO-glass substrate using convective assembly. The microspheres coating was done at a coating speed of 0.11-0.12 mm/s with a dispersed volume of 30-35µl with same particle concentration (7%-9%). Uniform close packed monolayer was obtained on most of the substrate area, with few multilayers and small voids, as observed with Nikon optical microscope shown in figure 3.6 (a).

Figure 3.5 Nikon Optical microscope

After the formation of monolayer with microspheres, spin-on-glass (SOG) was spin coated at 1000 rpm for 30 sec and heated on a hot plate at 90-100^{o}C in air for 1 to 2 minutes to remove any solvent and to cross link the SOG film. Closely bonded microspheres can be seen with few void spaces as observed with Nikon optical microscope shown in figure 3.6

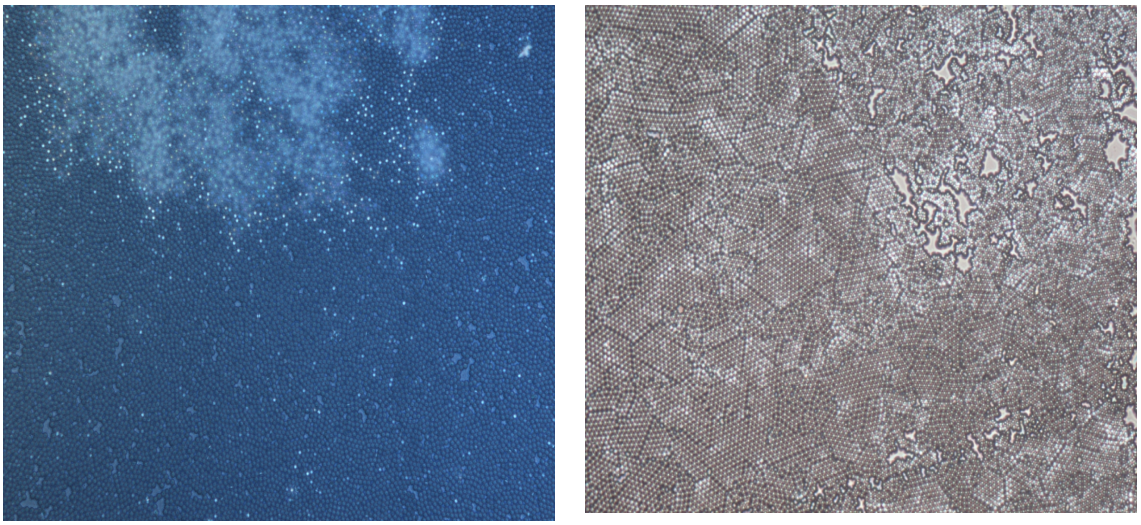

(a) (b)

Figure 3.6 Nikon Optical microscope images at 50 X magnification of (a) 2 µm silica microspheres and (b) after SOG film deposition

3.2 Fabrication of Organic Solar Cell

The hole conductive PEDOT: PSS (Poly (3, 4-ethylenedioxythiophene) poly (styrenesulfonate)) polymer was used as purchased from Sigma Aldrich^{R} without any further purification, the electron donor P3HT (poly 3-hexylthiophene) and electron acceptor PCBM (phenyl-C61-butyric acid methyl ester) was purchased from Sigma Aldrich^{R}. The active layer was prepared by mixing P3HT and PCBM in chlorobenzene at 1:1 ratio and stirred well in ultra sonicator until the best condition is achieved.

Figure 3.7 Picture showing PEDOT: PSS (left) and blend of P3HT and PCBM in chlorobenzene

After the omni-AR coating on the glass side of the substrate, PEDOT: PSS is dispersed with a syringe through a micro filter and spin coated at 3500 rpm for 40 sec and annealed at 90-100^{o}C on a hot plate for 10-15 minutes .The active layer is then spin coated at 850 rpm for 45 sec and then annealed at 90-100^{o}C for 20-30 min. The edges were cleaned with a solvent (chlorobenzene) for good contact during characterization. A tape is used as shadow mask to achieve desired active area and aluminum electrode is deposited using NRC thermal evaporator (figure 3.8) at a pressure of 10^{-6} torr. The sequence of device fabrication is shown in figure 3.9.

Figure 3.8 NRC Thermal Evaporator in NanoFab facility

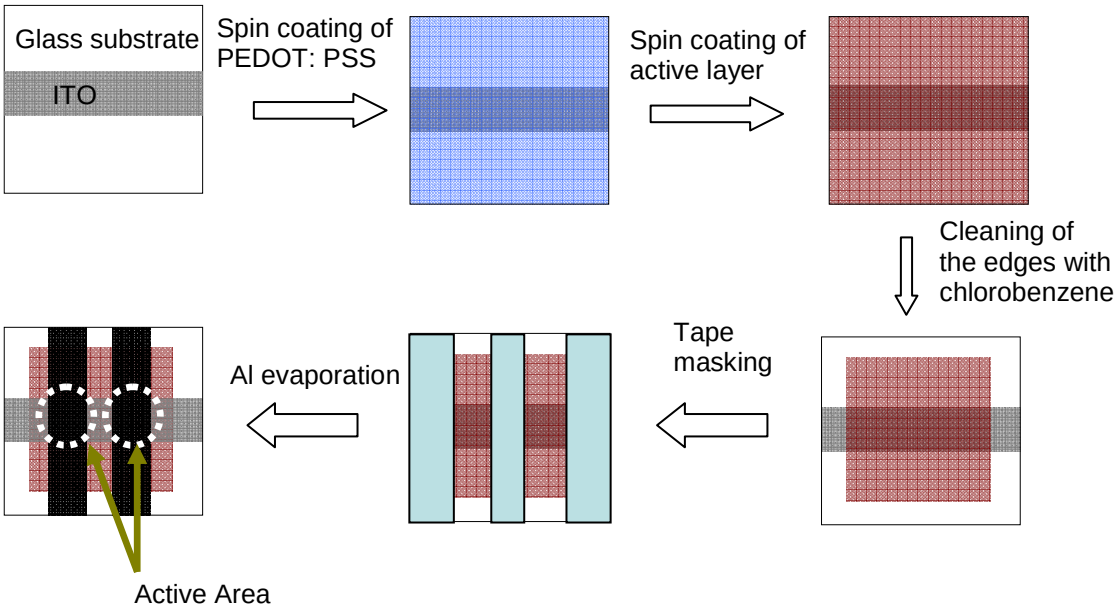

(a)

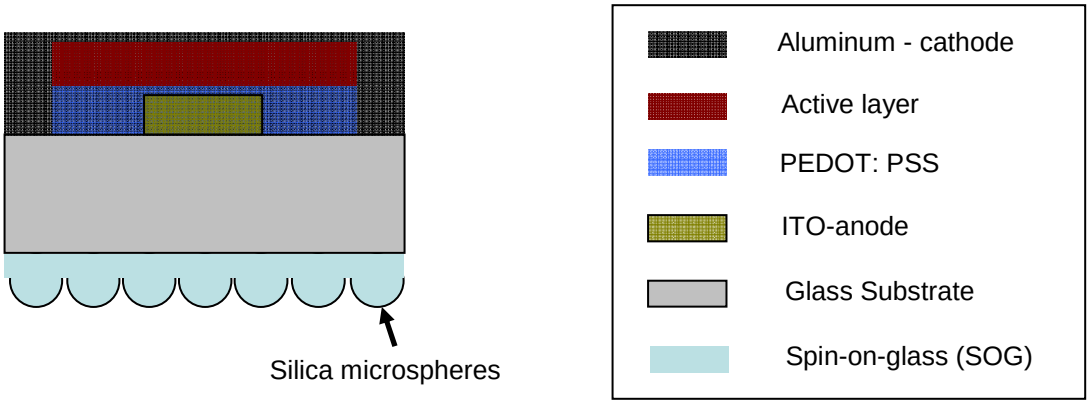

(b)

Figure 3.9 (a) Fabrication process (top view) of organic solar cell (b) Cross section of the fabricated organic solar cell

Four devices were fabricated, two each on a substrate with an active areas of around 0.12cm^2 and 0.25 cm^2 as shown in figure 3.10

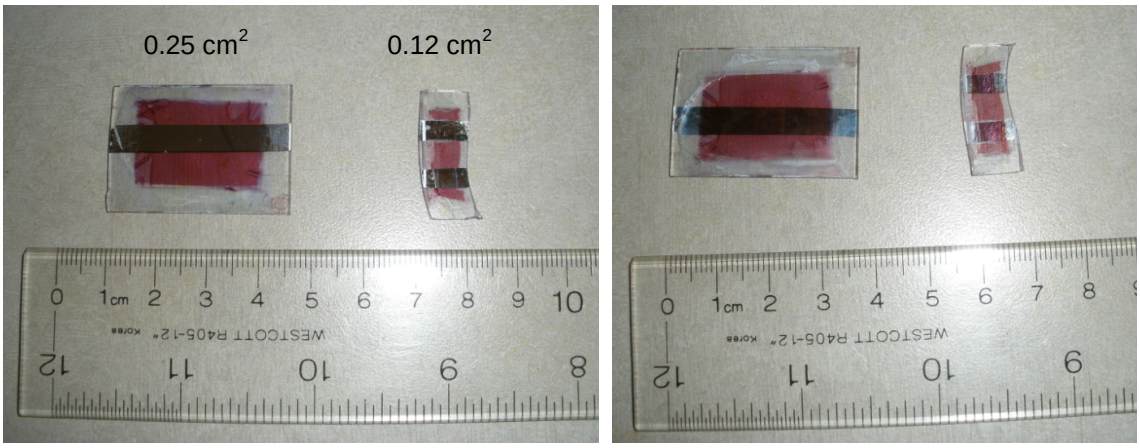

Figure 3.10 Pictures of organic solar cell on both sides of the device

3.3 Characterization and Discussion

The optical characteristics of an ITO-glass substrate with and without omni-AR coating are measured using UV/VIS spectrophotometer (JASCO V-570, Jaso Corp., Japan) over the spectral range of 400-1200 nm. The prolonged annealing effect of SOG at 90-100^{o}C was studied. It was found that there is no change in reflectance with omni AR coating after annealing for 2 min, 30 min and one hour (figure 3.11). This helped during organic solar cell fabrication where annealing at 90-100^{o}C is required during device fabrication without damaging the omni AR coating. This also proved that SOG acts as a strong bond between microspheres irrespective of any high temperature effects. The normal incident reflection and transmission of the ITO-glass substrate with and without omni-AR coating is shown in figure 3.12

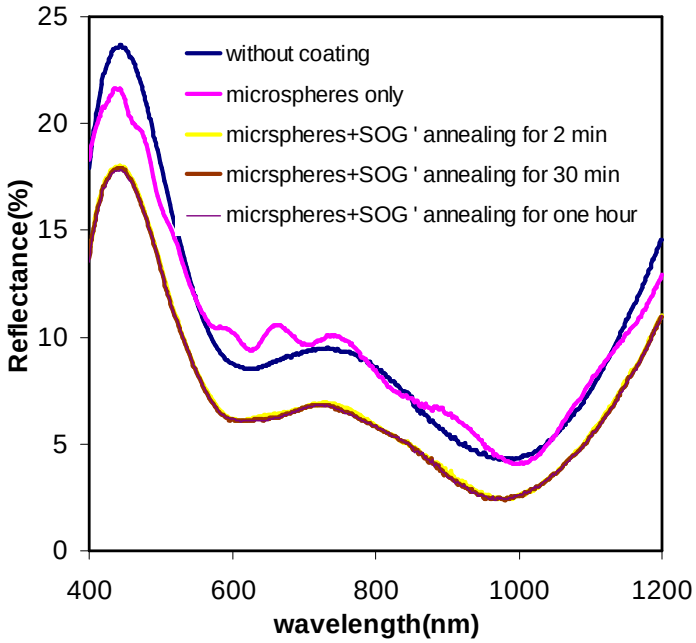

Figure 3.11 Measured reflectance for without omni AR and with omni AR coating at prolonged annealing times

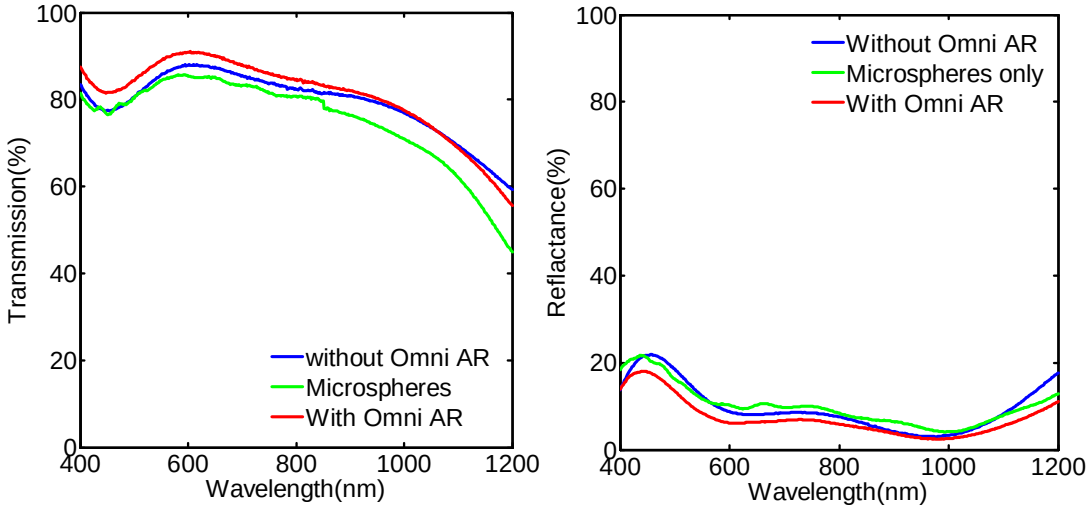

Figure 3.12 Measured transmission and reflection of ITO-glass substrate for without Omni AR coating, Microspheres only and with omni AR coating

There is a decrease in transmittance with only microspheres coating, this can be attributed to the presence of multiple surfaces in the spherical micro particle, and the deposition of spin-on-glass increased the transmission by reducing the number of surfaces to form hemispherical structure. The transmittance with omni-AR increased especially in the shorter wavelength whereas there is a little change at longer wavelength. In case of reflectance in the entire spectra there is a reduction in reflection. The current–voltage characterization was done with air mass1.5 (Appendix B) solar simulator, with xenon lamp as the light source. The power supply is set at 300 W, 15 Amps and 20 volts. Angle dependency set up was made to test the solar cell at different angles. Even though four probe testing can be done 2 probe crocodile clips were used because of the smaller size of the devices as shown in figure 3.13 and 3.14. The omni-AR coating was removed with hydrofluoric acid using cotton sticks in order to characterize the solar cells without omni-AR coating.

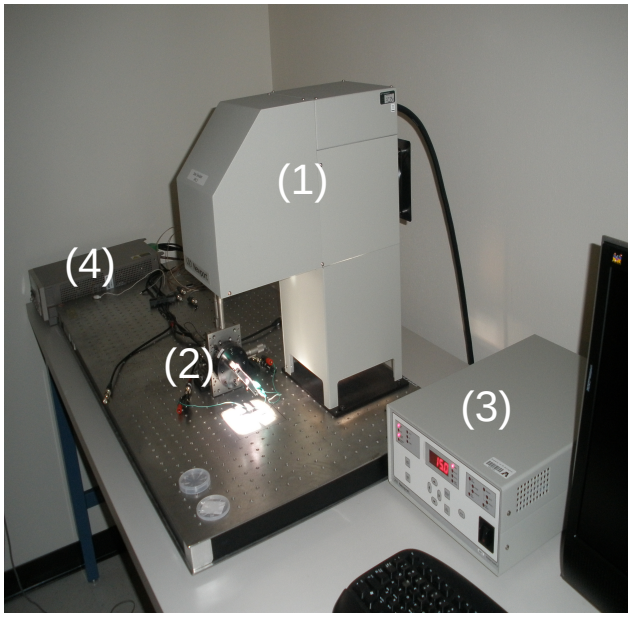

Figure 3.13 AM1.5 solar simulator with xenon as light source.(1) AM1.5 solar simulator (2) Angle dependency set up; 45 deg incidence shown as an example (3) power supply (4) Keithley 2601 source meter

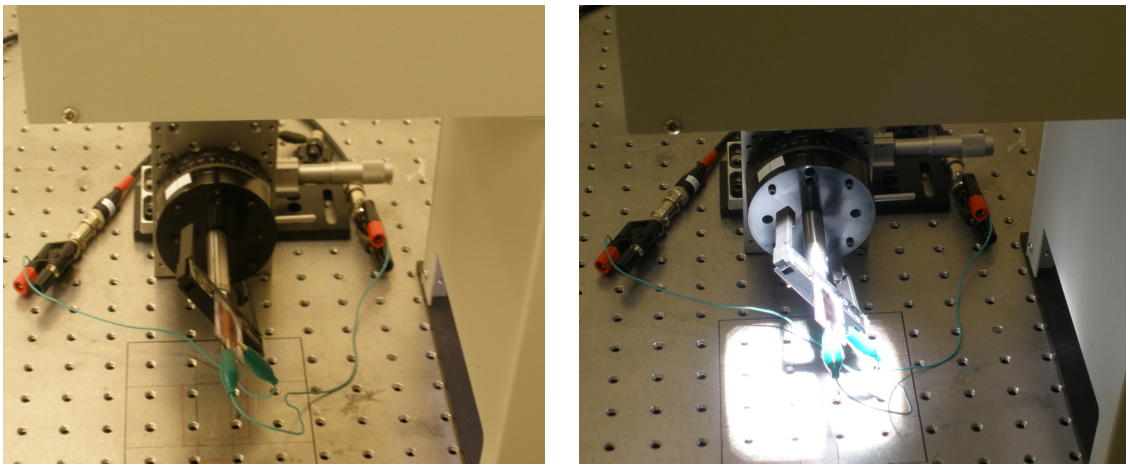

(a) (b)

Figure 3.14 2 * 2 inch^2 working plane with angle dependency setup showing 45 deg as an example (a) at dark condition (b) at illumination

The current –voltage characteristics of a typical organic solar at different angles of light incidence is shown in figure 3.15.

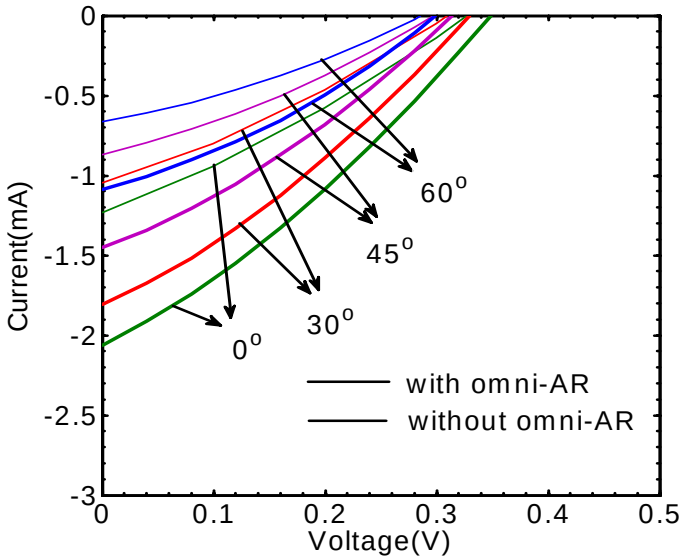

Figure 3.15 Measured Current-Voltage characteristics at surface normal, 30 deg, 45 deg and 60 deg with AM1.5 solar simulator

From the I-V curve there is a little change in the open circuit voltage with a significant increase in the short circuit current at all angles. This can be attributed to the increased light coupling due to omni AR coating and absorbance in the active area. The increase is more at smaller angle of incidence with maximum efficiency enhancement of around 70% at 30 deg angle of incidence. At larger angles there could be more photo light absorbance at ITO – glass substrate where holes are collected and apparently the absorption decreases in the active layer where excitons are generated. The solar cell parameters Isc, Voc and Pmax are shown in figure 3.16. The efficiency enhancement and relative efficiency enhancement for the set of 4 samples is shown in figure 3.17, the square symbol indicates the mean value of the four samples.

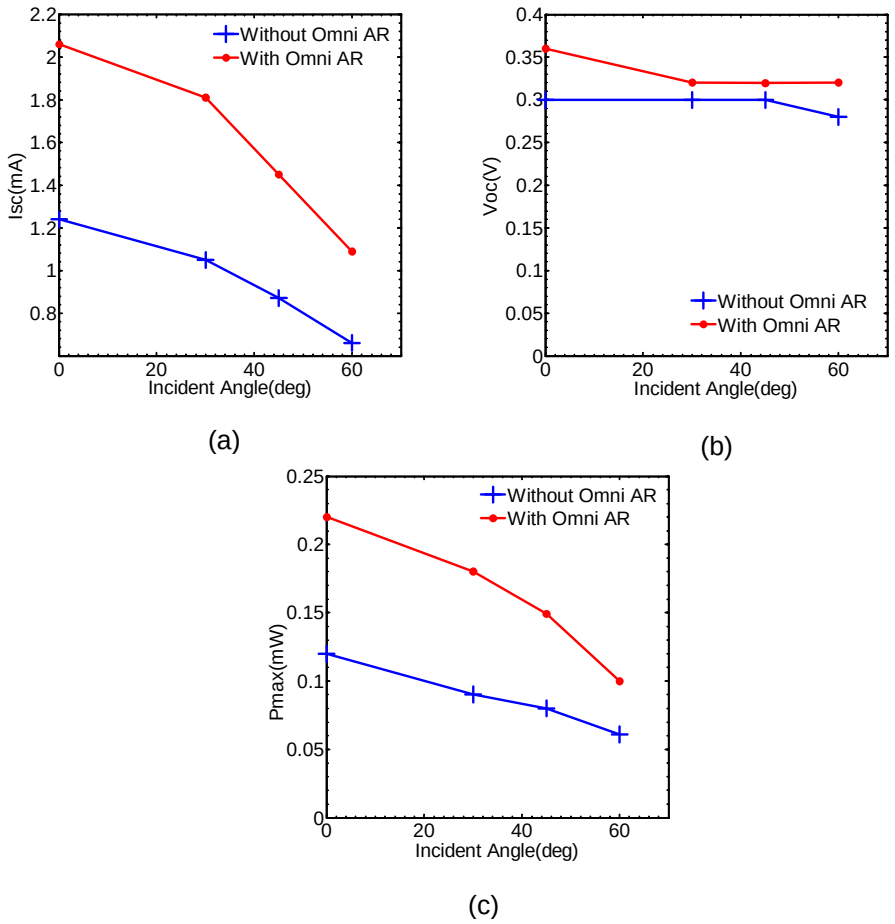

Figure 3.16 Solar cell parameters as a function of incident angle (a) short circuit current (b) open circuit voltage (c) maximum power output

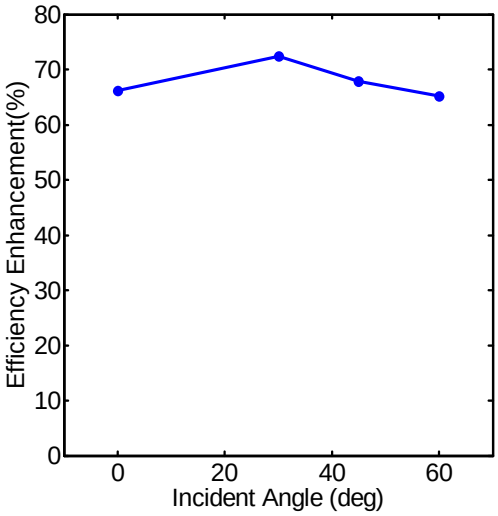

(a)

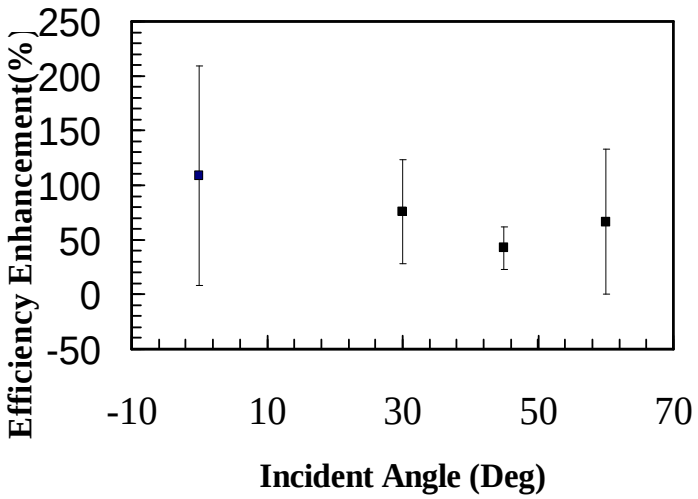

(b)

Figure 3.17(a) Relative efficiency enhancement as a function of incident angle for organic solar cell with the Omni-AR coating (b) Statistics of relative enhancement in efficiency as a function of incident angle for four organic solar cells with the omni-AR coating

CHAPTER 4

CONCLUSIONS

4.1 Summary

Convective coating and dip coating techniques were studied for depositing inorganic colloidal particle. Convective coating method was used for depositing solution processed omni-directional anti-reflection coatings on commercial amorphous silicon solar cells and on fabricated organic solar cells to improve the performance. Spherical textures are formed with 2 micron silica particles followed by spin coating process to deposit of spin-on-glass (SOG). The spherical texture reduced the reflectivity of the cells in the wavelength regime of 400-1200 nm, resulting in broader solar spectrum utilization. Angle dependency current-voltage characteristics from 0^o to 60^o were carried out to evaluate the performance of solar cells. Simulated reflectivity and efficiency enhancement results for commercial amorphous silicon solar cells were compared with measured values and found convincingly good agreement. Maximum relative efficiency enhancement was found to be 12% at 60^o of light incidence. The dip coating method was studied by depositing nano scale inorganic particle to obtain Distributed Bragg Reflectors (DBR) and its properties such as reflection and structural properties were analyzed.

4.2 Future Work

It is necessary to carry out more omni directional anti-reflection coatings using convective assembly on fabricated organic solar cell or on commercial organic solar cells in order to understand and validate the efficiency enhancement of the device. In the case fabricated Distributed Bragg Reflectors (DBR) there is a decrease in peak reflectivity at a particular wavelength after certain periods of deposition using dip coating, further study and understanding of different parameters involving the dip coating process need to be continued.

APPENDIX A

RELATION BETWEEN DISPLAY SPEED AND REAL SPEED FOR DIP COATING PROCESS

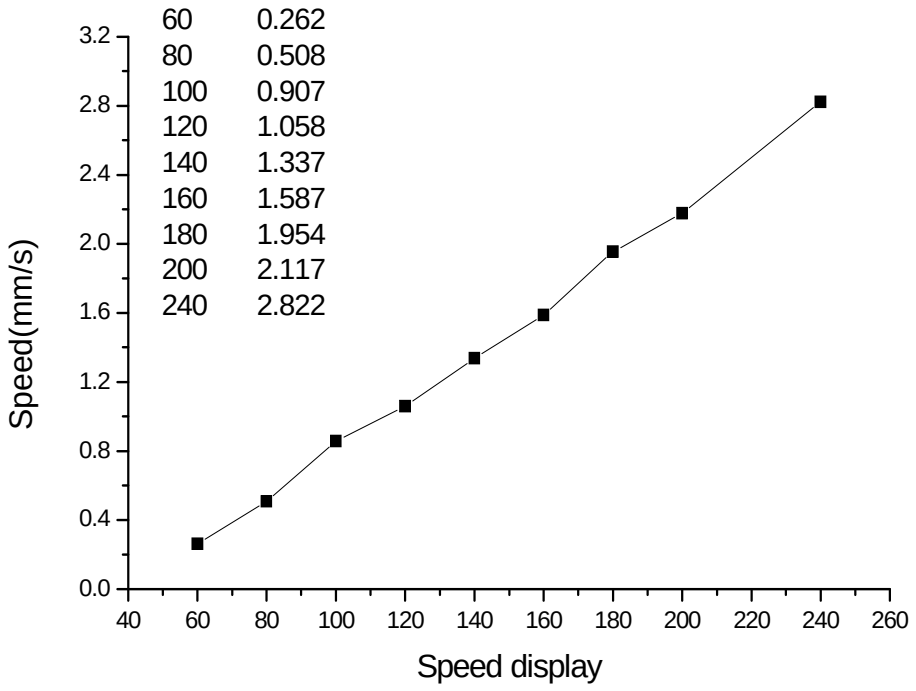

Figure A.1 Relation between Display Speed and Real Speed for Dip Coating Process

APPENDIX B

AIR MASS

Efficiencies for solar cells are usually given using AM 1.5 (Air Mass 1.5) solar illumination, where AM 0 is equivalent to solar illumination at the top of the atmosphere (i.e. in orbit), AM 1 is solar illumination at the earth' surface with sun directly above, AM 1.5 is on the earth's surface with the sun at 48.2^{o} angle and AM 2 is with the sun at a 60.1^{o} angle from vertical. Figure B.1 shows the relative solar illumination at different angles with respect to the sun.

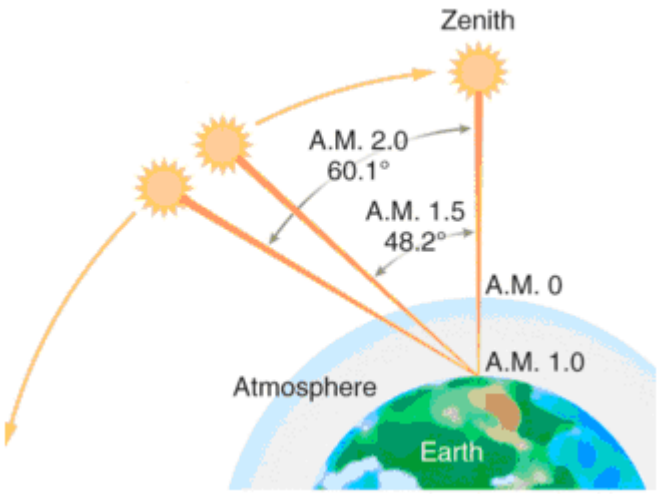

Figure B.1 Illumination levels at different angles.

REFERENCES

1. Meng Tao, Weidong Zhou, Hongjun Yang, Li Chen, “Surface texturing by solution deposition for omni directional antireflection”. Applied Physics letters, 91, 081118 (2007).
2. Weidong Zhou, Meng Tao, Li Chen and Hongjun Yang,” Micro structured surface design for omni directional antireflection coatings on solar cells”. Journal of Applied Physics, 102, 103105 (2007).
3. Yuehui Wang, Rajesh Tummala, Li Chen, Lilly Q Guo, Weidong Zhou and Meng Tao,” Solution processed omni directional anti reflection coatings on amorphous silicon solar cells”. Journal of Applied Physics (Accepted, 2009).
4. Brian G.Prevo, Daniel M. Kuncicky and Orlin D.Velev, “Engineered depositon of coatings from nano-and micro-particles: A brief review of convective assembly at high volume fraction” Colloids and Surfaces A: Physicochem. Eng. Aspects 311 (2007) 2-10.
5. Brian G. Prevo, “Engineered deposition of functional coatings from micro and nano particles using convective assembly”.
6. N.D.Denkov, O.D.Velev, et al Langmuir, 1992, 8, 3183.
7. N.D.Denkov, O.D.Velev, et al. Nature, 1993, 361, 26.
8. Y.Wang, Li Chen, H.yang,Q.Guo,W.Zhou, M. Tao.,” Spherical antireflection coatings by large-area convective assembly of monolayer silica microspheres” Solar Energy Materials and Solar Cells. 93 (2009) 85-91.
9. Fowles, G.R. “Introduction to modern optics; 2nd ed.; Over publicatons, Inc., 1989.
10. Alfred Thelen, “Design of optical interference coatings”, McGRAW-HILL Book Company.
11. L. D. Landau, B. G. Levich, Acta Physiochim, U.R.S.S., 17 (1942) 42-54.
12. L.E.Scriven, Mater.Res.Soc.Symp.1221 (1988) 717.
13. L.D.Landau, B.G. Levich, Acta Physiochiu,U.R.S.S 17 (1942) 42.
14. A. Van Blaaseren, R. Ruel and P. Wiltzius, Nature, 385, 321 (1997).

15. S. E. Han, A. Stein and D. Norris, Phys. Rev. Lett. 99, 053906 (2007).

16. J. C. Night, J. Brogeng, T. A. Birks and P. S. J. Russel, Science, 282, 1476 (1998).

17. A. Cho, Science, 299, 1685 (2003).

18. J. H. Holtz and S. A.Asher, Nature, 389, 829 (1997).

19. B. G. Prevo and O. D.Velev, Langmuir, 20, 2099 (2004).

20. R. Micheletto, H. Fukuda and M. Ohtsu, Langmuir, 11, 33336 (1995).

21. A.S.Dimitrov and K.Nagayama, Langmuir, 12, 1303 (1996).

22. Gang Li, Vishal Shrotriya, Yan Yao, and Yang Yang, Journal of Applied Physics 98, 043704 (2005).

23. Yu,G.,Gao, J., Hummelen,J.C., Wudl,F., and Heeger,A.J., “polymer photovoltaic cells – Enhanced efficiencies via a network of internal donor-acceptor heterojinctions,’ Science, 270,PP. 1789-1791(1995).

24. Harald Hoppe and Niyazi Serdar Sariciftci, Organic Solar cells: An Overview, Material Research Society, Vol 19, No.7, Jul 2004.

25. Polymeri Photovoltaics, A Practical Approach, Frederik C. Krebs., SPIE PRESS, Bellington,Washington,USA..

26. Michael D. Irwin, D. Bruce Buchholz, Alexander W. Hains, Robert P. H. Chang, and Tobin J. Mark., 2008 by proceedings of The National Academy of Sciences of the USA.

27. E. D. Palik, Handbook of Optical Constants of Solid, (Academic, Orlando, 1985).

BIOGRAPHICAL INFORMATION

Rajesh Tummala was born in Vuyyuru, Krishna district in Andhra Pradesh, INDIA in 1982. He received his bachelor's degree in Metallurgical Engineering at National Institute of Technology, Warangal, a reputed engineering college in INDIA, in May 2004. He then joined MALCO; Vedanta Group of Industries, a leading producer of non-ferrous metals in INDIA, in June-2004 as a process engineer and continued till July 2007 before quitting to pursue higher studies in Master of Science in USA.

He joined in the Material Science and Engineering department at The University of Texas at Arlington in fall-2007 to obtain his masters degree. He started working in Photonics Device Group from May-2008 as a graduate research assistant under the supervision of Professor Weidong Zhou. After finishing the Masters degree he is looking to work in a solar or semiconductor related industry.